On the use of X-ray computed tomography for determining wood properties: a review[1]

Qiang Wei, Brigitte Leblon, and Armand La Rocque

Can. J. For. Res. Downloaded from www.nrcresearchpress.com by UNIVERSITETSBIBLIOTEKET I TRONDHEIM on 09/18/12
For personal use only.

Abstract: In several processes of the forest products industry, an in-depth knowledge of log and board internal features is required and their determination needs fast scanning systems. One of the possible technologies is X-ray computed tomography (CT) technology. Our paper reviews applications of this technology in wood density measurements, in wood moisture content monitoring, and in locating internal log features that include pith, sapwood, heartwood, knots, and other defects. Annual growth ring measurements are more problematic to be detected on CT images because of the low spatial resolution of the images used. For log feature identification, our review shows that the feed-forward back-propagation artificial neural network is the most efficient CT image processing method. There are also some studies attempting to reconstruct three-dimensional log or board images from two-dimensional CT images. Several industrial prototypes have been developed because medical CT scanners were shown to be inappropriate for the wood industry. Because of the high cost of X-ray CT scanner equipment, other types of inexpensive sensors should also be investigated, such as electric resistivity tomography and microwaves. It also appears that the best approach uses various different sensors, each of them having its own strengths and weaknesses.

Résumé : Plusieurs processus de l'industrie des produits forestiers exigent une connaissance approfondie des caractéristiques internes des billes et des planches dont l'acquisition nécessite des appareils à balayage rapide. Une des technologies potentielles est la tomodensitométrie (TDM). Notre article passe en revue les applications de cette technologie pour mesurer la densité du bois, faire le suivi de la teneur en humidité dans le bois et localiser les caractéristiques internes du bois, telles que la moelle, le bois d'aubier, le bois de cœur, les nœuds et les autres défauts. Il est plus difficile de mesurer les cernes annuels sur les images obtenues par TDM à cause de la faible résolution spatiale de ces images. Pour l'identification des caractéristiques des billes, notre revue montre que le réseau neuronal artificiel multicouche à rétropropagation est la méthode la plus efficace pour traiter les images obtenues par TDM. Il y a aussi certaines études qui tentent de reconstruire des images en trois dimensions à partir des images en deux dimensions obtenues par TDM. Plusieurs prototypes industriels ont été développés parce qu'il a été démontré que les tomographes médicaux ne sont pas appropriés pour l'industrie du bois. Étant donné le coût élevé des appareils de TDM, d'autres types de capteurs bon marché devraient être étudiés, tels que la tomographie de résistivité électrique et les micro-ondes. Il semble aussi que la meilleure approche consiste à utiliser plusieurs capteurs différents, chacun ayant ses forces et ses faiblesses.

[Traduit par la Rédaction]

Introduction

In current wood manufacturing operations, knowledge of wood characteristics and measurement of those characteristics are essential to ensure that the right fibre is directed to the appropriate wood manufacturing company at the right time and cost to produce products in demand. Among all of the quality-related wood properties that should be monitored, density and moisture content are two of the most important because they affect the efficiency of manufacturing processes. For example, moisture content should be known to optimize the drying process or log inventory management. Density is related to stiffness and can be used to maximize fibre quality when bucking. Also, knowledge of the position and size of internal log defects, such as knots and decay, is required for optimizing log sawing that brings lumber value improvement, ranging from 3% to 28% depending on the species (Peter 1962, 1967; Wagner et al. 1989; Guddanti and Chang 1998; Schmoldt et al. 2000*b*; Lemieux et al. 2002; Rinnhofer et al. 2003).

To accurately control product quality before or during processing, there is the need of nondestructive real-time scanning of both the macroscopic and microscopic structure of wood properties. According to Bucur (2003*a*), knots and defects constitute the macroscopic structure of logs, while the microscopic structure of the wood is constituted by length, diameter, and shape of the tracheids, which are related to wood density and stiffness. Currently, there are several nondestructive technologies that use X-ray, gamma-ray, neutron, optical (visible and near- or shortwave infrared), thermal in-

Received 25 November 2010. Accepted 21 June 2011. Published at www.nrcresearchpress.com/cjfr on 26 October 2011.

Q. Wei, B. Leblon, and A. La Rocque. Faculty of Forestry and Environmental Management, 28 Dineen Drive, University of New Brunswick, Fredericton, NB E3B 6C2, Canada.

Corresponding author: Brigitte Leblon (e-mail: bleblon@unb.ca).

[1]This article is a contribution to the series The Role of Sensors in the New Forest Products Industry and Bioeconomy.

Can. J. For. Res. Downloaded from www.nrcresearchpress.com by UNIVERSITETSBIBLIOTEKET I TRONDHEIM on 09/18/12
For personal use only.

frared, microwave, ultrasound, radiofrequency, and magnetic resonance radiations. To reach deep wood layers, the radiation should have either a wavelength that is long enough or an energy that is high enough to penetrate the material. Microwave, ultrasound, and magnetic resonance radiations have wavelengths that are long enough (on the order of 10^{-2} m) to penetrate the wood material, but at the same time, they are not able to detect microscopic wood structures (Bucur 2003*a*). By contrast, X-ray, gamma-ray, and neutron radiations have a wavelength that is short enough (less than 10^{-9} m) to detect not only macroscopic but also submicroscopic and microscopic wood structures (Bucur 2003*a*). At the same time, these short-wavelength radiations have energy that is, according to the Plank's law, higher than 100 eV. This is enough to penetrate the wood material. Among all of the short-wavelength radiations, X-ray radiation is the most applicable (Osterloh et al. 2007). Other radiations require special equipment or settings, as they are produced by isotopes having a long life time. Compared with fast neutron technologies, X-ray-based technologies still deliver images of better quality and can be adopted for portable devices that can easily be taken onto sites (Osterloh et al. 2007).

Principles of X-ray ccanning computed tomography technology

X-ray scanners follow the theorem of Radon (1917) who theoretically demonstrated that the internal structures of an object can be reconstructed from single or multiple projections of the object, depending on the number of directions considered. Whatever the numbers of directions, X-ray beams are sent and detectors measure the X-ray radiation that is transmitted through the object (Fig. 1). The transmitted X-ray radiation can be related to the attenuation coefficient of the X-ray by the object by the Lambert–Beer exponential law under the assumption of a monochromatic ray and a linear propagation of the beam in the object (Davis and Wells 1992; Lindgren et al. 1992; Bucur 2003*a*):

$$[1] \qquad I = I_0 e^{-\mu d}$$

where I is the intensity of the transmitted X-ray beam passing through the object, I_0 is the intensity of the incident X-ray beam, e is Euler's constant = 2.718, d is the thickness of the object (length unit), and μ is the linear attenuation coefficient of the material along the transmission path (length unit^{-1}).

Single- or multidirectional industrial X-ray scanners have been developed for wood scanning (e.g., Oja et al. 2004; Grönlund et al. 2005), such as X-Scan (Luxscan), Denscan (MiCROTEC GmbH), and Goldeneye (MiCROTEC GmbH) for lumber scanning and OPMES AX1 (Mikropuu Oy), Wood X (Bintec Oy), ACTIS (Bio-Imaging Research), TOMOLOG and LOGEYE 301/306 (MiCROTEC GmbH), RemaLog XRay (RemaControl AB), and Pantak 420k-V (Omega International Technology Inc.) for log scanning. These scanners are based on digital radiography technology, which has several limitations (Harding et al. 2007). It was shown to be inappropriate for high moisture content logs, such as slash pine (*Pinus elliottii* Engelm.) logs (Harding et al. 2007). Indeed, thick layers of wood have the property to produce scattered radiation (particularly in the case of high moisture content) that renders the radiography noisy, making the perception of details difficult (Osterloh et al. 2006). Single-directional X-ray digital radiography scanners have the following additional drawbacks: (*i*) there are cases where feature location cannot be done along the X-ray path (Fig. 2*a*), (*ii*) the effects of high-density areas such as knots can be canceled out with effects of low-density areas such as cracks (Fig. 2*b*), and (*iii*) multiple dense areas may appear as a single dense area (Fig. 2*c*). While being used worldwide, both single- and multidirectional X-ray scanners do not have the high image resolution of computed axial tomography (CAT or CT) scanners that allow accurate analysis of wood properties and structures and their distribution within logs or wood products (Osterloh et al. 2006), particularly when features to be identified are lacking in contrast with their surrounding (Harding et al. 2007). To achieve the same precision, hundreds of X-ray directional scanners would have to be used (Harding et al. 2007; Brüchert et al. 2008).

Fig. 1. Principles of X-ray scanning. (Courtesy of Z. Pirouz, FPInnovations.)

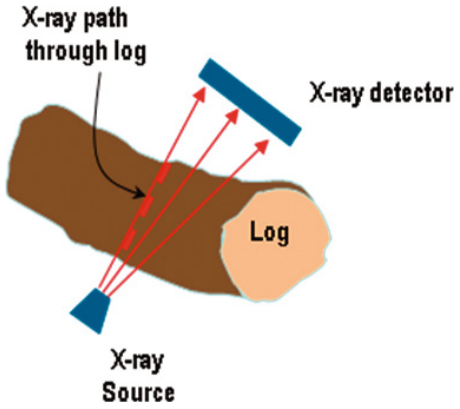

In the CT system, the X-ray tube rotates perpendicular to the longitudinal axis of the object through a full 360° arc with a wide fan beam. As the fan beam revolves, it activates those detectors that fall within its view on the opposite side of the object. After the rotation is completed, a computer calculates the X-ray absorption coefficient (μ) in small volume elements (voxels) within a slice. The calculated X-ray absorption coefficient in each voxel is normalized to the corresponding absorption coefficient for water to give the CT number, or Hounsfield number (H), according to the following scale (Benson-Cooper et al. 1982; Lindgren 1991*a*, 1991*b*; Davis and Wells 1992; Lindgren et al. 1992; Bucur 2003*a*):

$$[2] \qquad \text{CT number} = H = 1000 \times (\mu_x - \mu_{\text{water}})/\mu_{\text{water}}$$

where μ_x is the linear absorption coefficient for the tested wood material (length unit^{-1}) and μ_{water} is the linear absorption coefficient for the water (length unit^{-1}).

Equation 2 is usually used for medical CT scanners that typically have a mean photon energy around 73 keV. According to eq. 2, H varies from –1000 for air to +1000 for a material that has a density exactly twice the attenuation of water, H of water being 0. Because H is generally negative, an offset (of 1000, 1024, or 1035) is sometimes added to the original H values to obtain only positive values in the CT images (Lindgren et al. 1992; Longuetaud et al. 2005; Wei et al.

Can. J. For. Res. Downloaded from www.nrcresearchpress.com by UNIVERSITETSBIBLIOTEKET I TRONDHEIM on 09/18/12
For personal use only.

Fig. 2. Problems occurring with single-directional X-ray scanners, (*a*) The feature cannot be located along the X-ray path, (*b*) the effects of high-density areas such as knots can be canceled out with the effects of low-density areas such as cracks, and (*c*) multiple dense areas may appear as a single dense area. (Courtesy of Z. Pirouz, FPInnovations.)

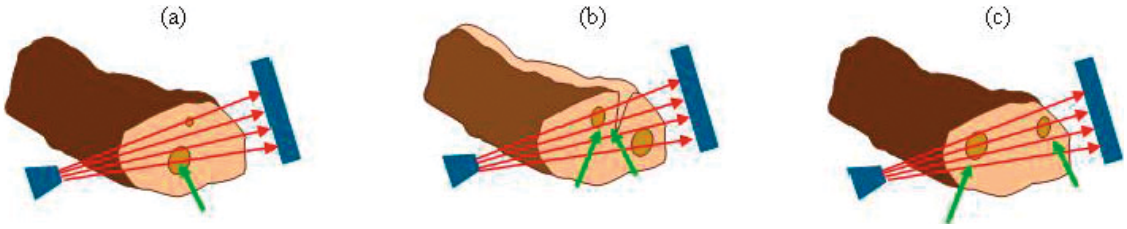

2008*a*; Hou et al. 2009). Typical *H* values of wood are given for a variety of tree species in Mull (1984), Klein and Vogel (1993), and Bucur (2003*a*). The *H* values corresponding to each voxel are then used to reconstruct the CT image, which is a matrix made by discrete picture elements (pixels) for which each gray-level (GL) value is proportional to the pixel *H* value that is related to the attenuation coefficient of the corresponding voxel. The voxel size is determined by the pixel size and the thickness of the X-ray beam. From separately successive scanned CT images, or "slices", it is then possible to reconstruct the entire log using three-dimensional (3D) reconstruction techniques (see "3D reconstructions" section below). Wood *H* values depend on wood density because the attenuation coefficient μ is directly related to density (cf. Tsai and Cho 1976; Lindgren 1991*a*, 1991*b*; Davis and Wells 1992; Macedo et al. 2002; Bucur 2003*a*). For this reason, the first application of CT images in the wood industry is to monitor wood density. CT images can also be used to image wood moisture content distribution because wood density highly depends on its moisture content (e.g., Simpson 1993). Each internal wood feature, such as defects, decay, heartwood, and sapwood, has a typical density and moisture content, so they appear differently on CT images, which can be used for feature detection.

Our study presents a review of the state of the art on the use of CT images for determining the following wood properties: (*i*) wood density, (*ii*) wood moisture content, and (*iii*) internal log features. Our review is an update of the reviews of Pham and Alcock (1998), Müller and Teischinger (2001), Bucur (2003*a*, 2003*b*), and Brashaw et al. (2009), but in contrast with these general reviews dealing with all existing nondestructive techniques applied to wood, our review has a special focus on X-ray CT image applications. It also compares the various image processing methods that were developed for processing CT images. A discussion about the operational use of X-ray CT scanners in the wood industry are also presented.

Wood density

Equation 2 gives the relationship between *H* and μ of the scanned material. In the model of Tsai and Cho (1976), the linear attenuation coefficient μ is the sum of two absorption coefficients, each of them being directly proportional to the material density ρ. Several other authors suggested that the linear attenuation coefficient μ can be directly related to the material density ρ as follows (Knoll 1989; Davis and Wells 1992; Wang 1997; Macedo et al. 2002; Bucur 2003*a*):

$$[3] \qquad \mu = \mu_m \times \rho$$

where μ is the linear attenuation coefficient of the material (m^{-1} or cm^{-1}), μ_m is the mass attenuation coefficient of the material ($m^2 \cdot kg^{-1}$ or $cm^2 \cdot g^{-1}$), and ρ is the material density ($kg \cdot m^{-3}$ or $g \cdot cm^{-3}$).

Combining eqs. 2 and 3 shows that *H* strongly depends on material density ρ. The other factors involved are the chemical composition of the material (Tsai and Cho 1976; Lindgren 1991*a*; Rojas et al. 2005; Freyburger et al. 2009) and the incident beam energy that is related to the type of scanner used (Macedo et al. 2002; Bucur 2003*a*; Freyburger et al. 2009). All of these factors are not independent. Material density ρ has the main influence for high-energy X-ray beams, whereas chemical composition has the main effect at low energy (Macedo et al. 2002; Freyburger et al. 2009).

The absolute values of *H* may vary significantly, even between two scanners of the same manufacturer and model (Levi et al. 1982; Mull 1984; Lindgren 1988, 1991*a*). Because of the unreliability of the absolute values of *H*, there is the need to calibrate CT scanners in terms of comparable quantities, such as the material density (Mull 1984). Two types of density can be defined for wood. The first one is green density that is computed as the green mass to green volume ratio. The second one is basic (dry) density that is computed as the oven-dry mass to green volume ratio. Linear relationships have been developed between H values and either green density (Table 1) or dry density (Table 2). Most of these relationships have been used as calibration curves for a specific scanner and thus were derived for a variety of tree species. Overall, relationships with density related to wood samples having some moisture content (either green density or air-dried density of samples having A moisture content around 12%) are better than relationships established with oven-dried samples because of the positive influence of moisture content. The relationship with the oven-dry density was insignificant in the case of the *Agathis* species in Hattori and Kanagawa'S (1985) study. Benson-Cooper et al. (1982) suggested including moisture content in the regression for estimating dry density from *H* values.

The influence of moisture content on *H* (and thus on the linear attenuation coefficient μ) should be related to its influence on the density (ρ) rather than on the mass attenuation coefficient μ_m (eq. 3). Gierlik and Dzbenski (1996) found an insignificant relationship between moisture content and μ_m. Lindgren (1991*a*) showed that *H* increases with increasing amount of water in a wooden test piece because of change in density. Indeed, the volume of air is being replaced by water, and according to eq. 2, water has a higher *H* value ($H = 0$) than air ($H = -1000$). The strong relationship between *H* and green density led some authors to consider that *H* values can

Can. J. For. Res. Downloaded from www.nrcresearchpress.com by UNIVERSITETSBIBLIOTEKET I TRONDHEIM on 09/18/12
For personal use only.

Table 1. Parameters for the linear relationship ($\rho = a \times H + b$) between green wood density (ρ) and the Hounsfield number (H).

Scanner	Energy (kV_{peak})	Intensity (mA)	Average energy (keV)	Species	Moisture content	a	b	R^2	n	Estimation error ($kg \cdot m^{-3}$)	Reference
Technicare Delta 2020	120	40–200 (during 2s)		5 species[a]	Green wood	0.910	1002	0.92	40		Benson-Cooper et al. 1982
Ohio Nuclear 2010	120	50 during 4 s		*Quercus* sp.	Green wood	1.043	1055	0.99		4	Mull 1984
				Black walnut (*Juglans nigra* L.)	Green wood	1.043	1055	0.99		7	
				6 species[b]	Green wood	1.043	1055	0.99	6	8.7	
EMI CT1010	120	20–30	70	12 species[c]	Green wood	1.006	1035	na	13	na	Davis and Wells 1992
Toshiba TCT-20 A	120			*Shorea* sp.	2%–96%	1.002	1018	0.98	35		Hattori and Kanagawa 1985[d]
				Agathis sp.	2%–27%	0.894	966	0.94	35		
GE 9800 Quick	120	70	73	Scots pine (*Pinus sylvestris* L.)	6%–117%	0.993	1015	na	50	13.4	Lindgren 1991*a*
Siemens SOMATOM Plus 4 Volume Zoom CT	140	178		Balsam fir (*Abies balsamea* (L.) Mill.)	107.5%	0.860	1046	0.62	25	1–15	Hou et al. 2009
				Eastern beech (*Fagus grandifolia* Ehrh.)	68.5%	0.694	916	0.92	23	6–11	

[a]Radiata pine (*Pinus radiata* D. Don), Douglas-fir (*Pseudotsuga menziesii* (Mirb.) Franco), *Eucalyptus delegatensis* R. Baker, Tasmanian blackwood (*Acacia melanoxylon* R. Br.), red beech (*Nothofagus fusca* (Hook. f.) Oerst.).

[b]Pine (*Pinus* sp.), mahogany (*Swietenia mahagoni* (L.) Jacq.), poplar (*Populus* sp.), maple (*Acer* sp.), ash (*Fraxinus* sp.), teak (*Tectona* sp.).

[c]Balsa (*Ochroma pyramidale* (Cav. ex Lam.) Urb.), treated pine (*Pinus* sp.), radiata pine (*Pinus radiata* D. Don), Oregon, meranti (*Shorea bracteolate* Dyer), Cypress pine (*Callitris* sp.), merbau (*Intsia* sp.), New Zealand pencil pine (*Athrotaxis cupressoides* D. Don), red gum Jarrah (*Eucalyptus marginata* Donn ex Sm.), gray box, red box, red iron bark (*Eucalyptus fibrosa* F. Muell.).

[d]This study computes H as a function of ρ. The parameters a and b have therefore been recomputed from the published regression parameters. For the slope parameter, it is slightly different from what would have been obtained by estimating directly the a and b parameters. All of the wood samples were surrounded with granular sugar for improving the density uniformity of the CT image.

Can. J. For. Res. Downloaded from www.nrcresearchpress.com by UNIVERSITETSBIBLIOTEKET I TRONDHEIM on 09/18/12
For personal use only.

Table 2. Parameters of the linear relationship ($\rho = a \times H + b$) between the dry wood density (ρ) and the Hounsfield number (H).

Scanner	Energy (kV_{peak})	Intensity (mA)	Average energy (keV)	Species	Drying	a	b	R^2	n	Estimation error ($kg \cdot m^{-3}$)	Reference
Technicare Delta 2020	120	40–200		5 species[a]	Oven	—[e]	—[e]	0.82[e]	40		Benson-Cooper et al. 1982
Philips 210				Scots pine (*Pinus sylvestris* L.)	Oven	1.075	1076	0.98	7		Lindgren 1985[f]
GE 9800 Quick	120	70	73	Scots pine (*Pinus sylvestris* L.)	Oven	1.052	1053	na	11	4	Lindgren 1988
Toshiba TCT-20 A	120			*Agathis* sp.	Oven			ns	35		Hattori and Kanagawa 1985[f]
				Shorea sp.	Oven	0.973	1040	0.74	35		
Homemade	160	18.75	28.3	6 species[b]	Air	0.826	779	0.98	6		Macedo et al. 2002[g]
Medical CT scanner				Hardwood	Air	1.044	1044	0.99	25		Taylor 2006
GE Bright-Speed Excel	120	50		16 species[c]	Air	1.058	1062	0.99	16	4.5–8.0	Freyburger et al. 2009
	120	50		7 species[d]	Air	1.058	1062	0.99	21	5.4–7.7	

[a]Radiata pine *(Pinus radiata* D. Don), Douglas-fir (*Pseudotsuga menziesii* (Mirb.) Franco), *Eucalyptus delegatensis*, Tasmanian blackwood (*Acacia melanoxylon* R. Br.), red beech (*Nothofagus fusca* (Hook f.) Oerst.)

[b]white birch (*Betula papyrifera* Marsh.), *Liquidambar styraciflua* L., Douglas-fir (*Pseudotsuga menziesii* (Mirb.) Franco), red oak (*Quercus rubra* L.), western hemlock (*Tsuga heterophylla*), yellow-poplar (*Liriodendron tulipifera* L.).

[c]*Brosimum guianense* (Aubl.), *Dicorynia guianensis* (Amsh.), *Bocoa prouacensis* (Aubl.), *Hymenaea courbaril* (L.), *Parkia nitida* (Miq.), *Tabebuia serratifolia* (Vahl), *Qualea rosea* (Aubl.), *Sextonia rubra* (Mez), *Simarouba amara* (Aubl.), *Vouacapoua americana* (Aubl.), *Ochroma lagopus* (O.P. Swartz), *Peltogyne venosa* (Vahl), *Bagassa guianensis* (Aubl.), *Cecropia sciadophylla* (Mart.), *Diplotropis purpurea* (Rich.), *Aspidosperma album* (Vahl).

[d]*Peltogyne venosa* (Vahl), sessile oak (*Quercus petraea* (Mattuschka) Liebl.), Norway spruce (*Picea abies* (L.) Karst.), European beech (*Fagus sylvatica* (L.)), *Prunus avium* (L.), *Ulmus* sp., Scots pine (*Pinus sylvestris* (L.)).

[e]Multiple regression with the moisture content as second regressor.

[f]These studies computed H as a function of ρ. The parameters a and b have therefore been recomputed from the published regression parameters. For the slope parameter, it is slightly different from what would have been obtained by estimating directly the a and b parameters. The regression is not significant in the case of *Agathis* sp. For Hattori and Kanagawa's (1985) study, the wood samples were surrounded by granular sugar to improve the density uniformity of the CT images.

[g]The H values have been recomputed from the published linear attenuation coefficients using eq. 1.

Can. J. For. Res. Downloaded from www.nrcresearchpress.com by UNIVERSITETSBIBLIOTEKET I TRONDHEIM on 09/18/12
For personal use only.

be replaced by density values when analyzing CT images. For Longuetaud et al. (2005, 2007), 1 unit of H can be considered as being equivalent to a density of 1 kg·m^{-3}. CT images have been segmented based on density threshold values instead of H threshold values (Grundberg and Grönlund 1991; Longuetaud et al. 2005, 2007). However, one may pay attention to some limitations in using the H–ρ relationship. In the case of sugar maple (*Acer saccharum* Marsh.) logs, Rojas et al. (2005) scaled CT images into 256 GL images and showed that the relationship between GL values and the green density varies with the type of internal log feature considered (sapwood, knot, heartwood, knots). They hypothesized that this difference should be attributed to the state of crystalline structures in the different log features.

CT-derived wood density measurements are useful in wood biomass and carbon storage estimations (Freyburger et al. 2009) and in monitoring wood strength and wood stiffness. For example, Axelsson (1994) used CT images for studying momentary disturbances due to changes in the wood structure that can cause asymmetrical lateral forces and lateral deflexions of the saw tooth and saw blade. CT images have been used to assess the distribution of horizontal density in Chinese fir (*Cunninghamia lanceolata* (Lamb.) Hook.) oriented laminated stick lumber (Du et al. 2009). CT images were even used in forest management studies to determine the effect of thinning on density of Austrian pine (*Pinus nigra* Arnold) (Uner et al. 2009).

Because CT values are strongly related to green density, which is dependent on moisture content, one of the applications of CT images in the wood industry is for assessing moisture content distribution within logs or wood products (see next section). Another important industrial application of CT images is for identifying internal log features that differ based on their density or moisture content and thus on CT values (see "Identification of internal log features" section below). For this application, several factors should be considered when selecting the radiometric and spatial resolution of the CT images. With respect to the radiometric resolution, features are easily distinguished in CT images if they differ in density by 1%–2% (Schmoldt et al. 2000*b*) or by about 2 kg·m^{-3} in the case of basic densities and about 6 kg·m^{-3} in the case of green densities with moisture content levels ranging from 6% to 100% (Lindgren 1991*b*). With respect to the spatial resolution, Lindgren et al. (1992) was not able to measure density in earlywood or latewood of Scots pine (*Pinus sylvestris* L.) wood specimens because of the too coarse resolution of the CT image compared with the annual growth ring width. They suggested that density measurements using CT images can only be done over large uniform density areas. The density distinction capability of CT images was also found to be related to the scanned volume because the accuracy of wood density measurements was shown to be low for small volume size (Lindgren 1991*b*).

Wood moisture

Wood moisture is an important property to be measured and is highly related to wood density that can be monitored using CT images (see "Wood density" section above). One of the most important industrial applications of CT images is monitoring of wood moisture during the drying process. For modeling the kiln drying process of boards, CT images have been used to determine moisture flux and diffusion coefficients (e.g., Danvind and Morén 2004), to validate mathematical models in the case of radiata pine (*Pinus radiata* D. Don) (Pang and Wiberg 1998) or of Norway spruce (*Picea abies* (L.) Karst.) (Eriksson et al. 2007), to assess wet-wood distributions in heartwood in the case of subalpine fir (*Abies lasiocarpa* (Hook.) Nutt.) (Alkan et al. 2007), and to assess moisture content distribution, two-dimensional (2D) displacements, and related strains in the case of Scots pine (Danvind 2002; Danvind and Morén 2004). Outside of monitoring drying processes, CT images were also tested to assess moisture content distribution during microwave heating of Scots pine boards (Hansson and Antti 2008) and to describe water sorption in specimens made of Norway spruce wood (Sandberg 2006) or of European aspen (*Populus tremula* L.), English oak (*Quercus robur* L.), and Scots pine wood (Johansson and Kifetew 2010).

Wood moisture monitoring is also useful in tree physiology studies such as those related to water processes in trees. The first tree physiology studies used gamma-ray CT images, for example to relate sap flow to wood density, water content, and cavitations rate of sessile oak (*Quercus petraea* (Mattuschka) Liebl.) and Turkey oak (*Quercus cerris* L.) mature standing trees (Tognetti et al. 1996) and to study water stress on healthy and unhealthy trees of decaying oak forests (Fenyvesi et al. 1998) or following pollution over Scots pine trees (e.g., Lüttschwager et al. 2004). Nikolova et al. (2009) used X-ray CT images to study the role of sapwood and heartwood in the water transport of Norway spruce and oak (*Quercus* species) trees and to measure the conductive lumen area of coarse-root conduits in the case of European beech (*Fagus sylvatica* L.) and Norway spruce trees.

One of the problems of using CT images for moisture content distribution assessment is the interference with wood density. One may assume that the wood basic (dry) density profile is known (Pang and Wiberg 1998). Also, during wood drying, a change in wood volume (i.e., shrinkage) can occur. Considering the effect of drying on both wood volume and density, the method presented in Fig. 3 was developed for measuring strain and moisture content in a cross section of drying wood (Danvind 2002) and for assessing drying behaviour of knots and their surroundings (Danvind and Morén 2004) from CT images. The method considers the changes in both density and volume during drying.

Identification of internal log features

The internal log features that should be identified on a CT image include pith, growth rings, heartwood, sapwood, knots, and other defects such as decay.

Pith location

Most of the studies on automated detection of the pith on CT images are based on growth rings. For CT images of logs of radiata pine and eucalyptus (*Eucalyptus regnans* L. and *Eucalyptus marginata* L.), Som et al. (1993, 1995) created an edge image using the second-derivative operator or using top-hat morphologic operators. The pith was located using the ring tangents at 0° and 90°. All other growth ring based studies on the automated detection of the pith on CT images

Can. J. For. Res. Downloaded from www.nrcresearchpress.com by UNIVERSITETSBIBLIOTEKET I TRONDHEIM on 09/18/12
For personal use only.

Fig. 3. Flowchart of a method for estimating moisture content from CT images in a drying piece of wood (after Danvind and Morén 2004).

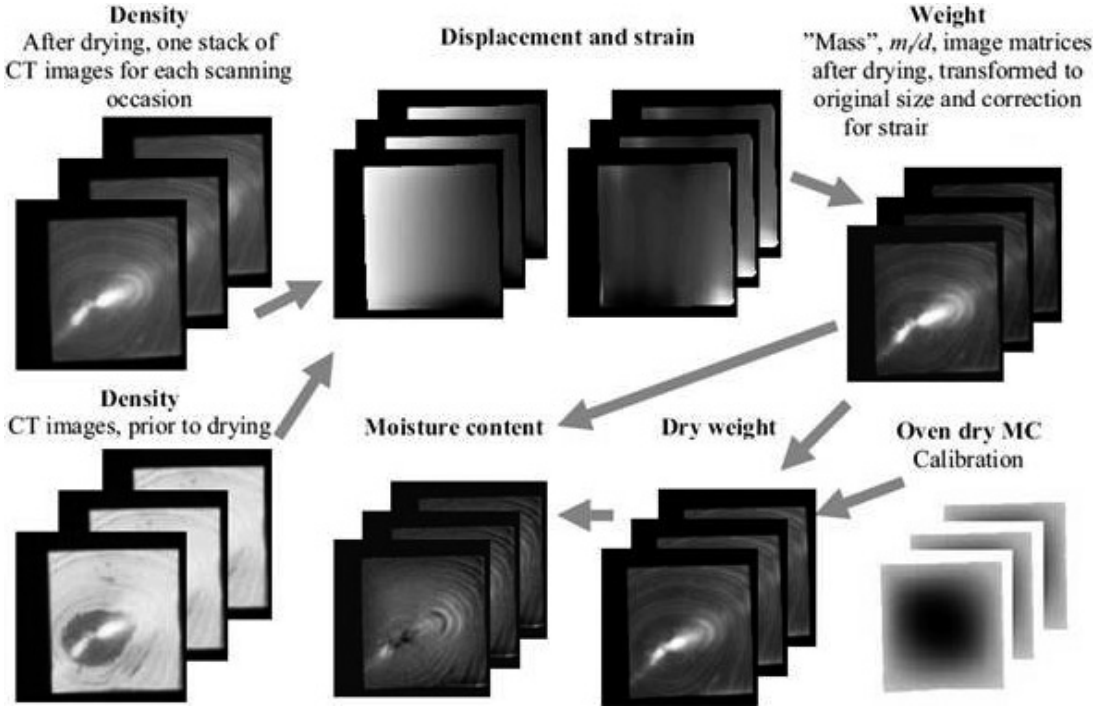

used the Hough transform (HT) method (Hough 1962) in the case of hardwood (Bhandarkar et al. 1999) or softwood tree species (Wu and Liew 2000; Andreu and Rinnhofer 2001; Longuetaud et al. 2004). The HT method supposes that the growth rings are circular and centered on the pith. First, the image is filtered using an edge operator (Sobel or Canny) to compute the gradient value and orientation. The resulting edge point image is then used to compute an HT accumulation image. The pith location is then derived as the coordinate corresponding to the maximum GL value of the HT accumulation image. Andreu and Rinnhofer (2001) used a different approach to create the HT image. First, they applied a Fourier transform in local neighbourhoods to compute frequency and orientation parameters. Each neighbourhood was filtered using a Gabor filter that was set on these parameters. The HT method was then used to exploit the fact that the line perpendicularly bisecting a chord passes through the center of the circle.

Some of the automated pith location methods do not use growth rings. For example, Jaeger et al. (1999) proposed a method of pith location on CT images acquired over Norway spruce logs that is based on the low density of the pith compared with the surrounding area, the pith being manually located on the first CT slice. Flood et al. (2003) based their algorithm on the branch orientation in the log using a 3D shape and direction discriminating method. Longuetaud (2005) compared the tangent-based method of Som et al. (1993, 1995), the density-based method of Jaeger et al. (1999), and an HT-based method (Wu and Liew 2000) and concluded that the HT-based method gives the best location accuracy.

Bhandarkar et al. (1999) suggested that a good pith location error should be around 10 pixels (7.5 mm). Som et al.'s (1993, 1995) method was tested over five images and the mean location error was 5.4 pixels (5.4 mm). Bhandarkar et al. (1999) achieved a location precision of 5 pixels (3.75 mm) for the majority of the processed CT images and a precision of 20 pixels (15 mm) for almost all of the processed CT images. The poorest accuracy was achieved for sugar maple logs and the best one for black walnut (*Juglans nigra* L.) logs. For Norway spruce logs, Andreu and Rinnhofer (2001) achieved a mean location precision of 2.2 pixels with a maximum error of 6.7 pixels on CT images acquired with an industrial CT scanner. With images acquired with a medical CT scanner, Longuetaud et al. (2004) were able to achieve an average pith location accuracy of less than 1 pixel (1 mm), with more than 95% of the images having a pith location error of less than 1.97 mm.

Growth rings

Medical or industrial X-ray CT images produce too coarse images and cannot be used for accurately measuring growth ring parameters. Lindgren et al. (1992) showed that medical CT images were not able to measure densities within growth ring structures, i.e., densities of earlywood and latewood, of Scots pine logs when the growth ring was smaller than 4 mm. Okochi et al. (2007) and Brüchert et al. (2008) reported that CT images cannot measure annual growth ring widths of less than 1 mm. For CT images acquired over Norway spruce logs, Jaeger et al.'s (1999) algorithm that automatically detected growth rings based on radii drawn from the pith did not work beyond the 15th to 20th growth ring because the rings have a too small width. Andreu and Rinnhofer (2001, 2003) applied a Fourier transform and a Gabor filter to enhance the visibility of growth rings over CT images to locate the pith of Norway spruce logs.

Other types of images have been used for growth ring studies, such as cross-section images (e.g., Sliwa et al. 2003), magnetic resonance images (Morales et al. 2004), X-ray analog radiography images (Parker and Jozsa 1973), X-

Can. J. For. Res. Downloaded from www.nrcresearchpress.com by UNIVERSITETSBIBLIOTEKET I TRONDHEIM on 09/18/12
For personal use only.

ray digital radiography images (Wang 1997), and X-ray microtomography (μCT) images (e.g., Lindgren et al. 1992; Okochi et al. 2007). These techniques are also used in dendrochronology studies and for dating heritage wood specimens (Okochi et al. 2007).

Heartwood and sapwood

Heartwood and sapwood are important to be discriminated in several applications. For example, in tree physiology studies, sapwood parameters were related to needle biomass (Gruber 1995) and were used to study water-related processes in trees (Fromm et al. 2001) or tree vitality or pollution impact (Lüttschwager et al. 2004). In industrial applications, heartwood and sapwood have different physical and technological properties, including colour, moisture content, durability, and suitability for chemical treatment (Panshin and de Zeeuw 1980; Björklund 1999; Oja and Temnerud 1999; Rojas et al. 2005, 2006, 2007). In log breakdown processes, there is the need to delineate heartwood–sapwood borders, either because heartwood is a defect, such as the coloured heartwood of the sugar maple (Rojas et al. 2006) or the defective core of pruned radiata pine (Benson-Cooper et al. 1982; Rojas and Ortiz 2009) or because knots are difficult to distinguish from sapwood over CT images (see "Other defects" section below).

Because heartwood and sapwood areas and widths are considered as wood quality parameters, some studies on the use of CT images in heartwood and sapwood identification attempted to directly relate heartwood and sapwood areas and widths to tree, stand, or site inventory variables. Sapwood width extracted from CT images acquired over Norway spruce logs were correlated with tree slendemess (tree height and breast height diameter) and with the relative height of the crown (Longuetaud et al. 2006). However, in the case of Scots pine, Björklund (1999) found that heartwood area percentage, heartwood radius, and sapwood width extracted from CT images of logs varied too much between individual trees and between stands to be significantly correlated with tree, stand, and site variables.

Heartwood generally has a higher moisture content and concentration of certain inorganic and extractive materials than sapwood (Rojas et al. 2005). Since water has a higher density than wood, regions of high moisture content such as heartwood will appear brighter in the CT image (Fig. 4*a*). However, there are species such as black spruce (*Picea mariana* (Mill.) BSP) for which the heartwood has a lower density and moisture content than the sapwood (Panshin and de Zeeuw 1980), so it will appear dark on the CT image (Fig. 4*b*). In both cases, because of the difference in density and (or) moisture content between heartwood and sapwood, CT images will thereby be suitable for distinguishing heartwood and sapwood. However, this difference is less strong over dry logs (Björklund 1999). For Scots pine logs, Grundberg and Grönlund (1991) used fixed GL threshold values, which are expressed in density values, to separate heartwood from sapwood, but the density thresholds cannot differentiate between heartwood and dead knots and between sapwood and sound knots. Grundberg and Grönlund (1992) delineated the border between heartwood and sapwood by applying GL-based thresholds on low-pass-filtered images and by computing gradient images using a Roberts filter to highlight the border between heartwood and sapwood. Such a method allows describing the heartwood–sapwood border by a mean radius for 12° sectors every 10 mm along the log that is expressed in polar coordinates originated from the pith. Grundberg and Grönlund's method was used in several studies (e.g., Hagman and Grundberg 1995; Björklund 1999; Chiorescu and Grönlund 2000). All of the methods developed by Grundberg and Grönlund did not take explicitly into account the knot disturbance of the heartwood–sapwood border. It is why Longuetaud et al. (2005, 2007) proposed an image processing method to delineate the heartwood–sapwood border for Norway spruce green logs, which also works for knotty CT slices as follows: (*i*) location of the pith by the method of Longuetaud et al. (2004), (*ii*) Gaussian smooth filtering to reduce the contrast between earlywood and latewood of annual rings in the heartwood, (*iii*) for each knot-free CT slice, drawing 360 radii every degree from the pith and computating the distance from the pith to the first pixel whose GL value exceeds 800 (representing the heartwood–sapwood boundary) (for CT slices with knots, the distance is computed from the pith to the knot and the resulting boundary is corrected in the next step, (*iv*) post-processing to delineate the heartwood–sapwood boundary in the area of knots by longitudinal interpolation of the boundary between CT slices of the same log, and (*v*) delineation of a continuous boundary for each CT slice by linearly joining the 360 points for each cross section. They achieved accuracy in the hardwood–sapwood boundary delineation of 1.8 mm on average.

In previous studies, image region identification through thresholds and labeling were done in two steps. This increases the computing time of the developed algorithms and thus their real-time operability. One way to achieve both image region identification and labeling in one step is through the Bayesian maximum likelihood classifier. Such a classifier was used to identify selected log features (sapwood, heartwood, knots, and bark) in CT images acquired over sugar maple logs (Rojas et al. 2006, 2007; Wei et al. 2008*a*) and over black spruce logs (Wei et al. 2009*a*, 2010). All of the studies first removed the air background from the images based on GL threshold values. While Rojas et al.'s studies used only the spectral information of the image, i.e., GL values, as input features in the classifier, Wei et al.'s studies also used variables that depend on the spatial information of the image, such as the Euclidean distance from the pith and seven textural features (homogeneity, contrast, dissimilarity, mean, standard deviation, entropy, and angular second moment) that were computed using the GL co-occurrence matrix method of Haralick et al. (1973). The classification producer's accuracies (as defined by Congalton 1991) for the sapwood and heartwood classes are compared for all of the Rojas et al. and Wei et al. studies in Table 3. Table 3 results show that for sugar maple logs, the classification was better for freshly cut logs than for logs that dried sometimes on the wood yard. Such better results can be explained by the positive influence of moisture content in identifying heartwood and sapwood over CT images. Rojas et al. (2007) even found a quadratic relationship between log moisture content and sapwood classification accuracies. As expected, applying the maximum likelihood classifier to validation CT images, i.e., those that were not used for training the classifier, reduced the class accuracies for both wood types and species (Ta-

Can. J. For. Res. Downloaded from www.nrcresearchpress.com by UNIVERSITETSBIBLIOTEKET I TRONDHEIM on 09/18/12
For personal use only.

Fig. 4. Comparison between a CT slice acquired over (*a*) a sugar maple (*Acer saccharum*) log and (*b*) a black spruce (*Picea mariana*) log (after Wei et al. 2008*a*, 2009*a*).

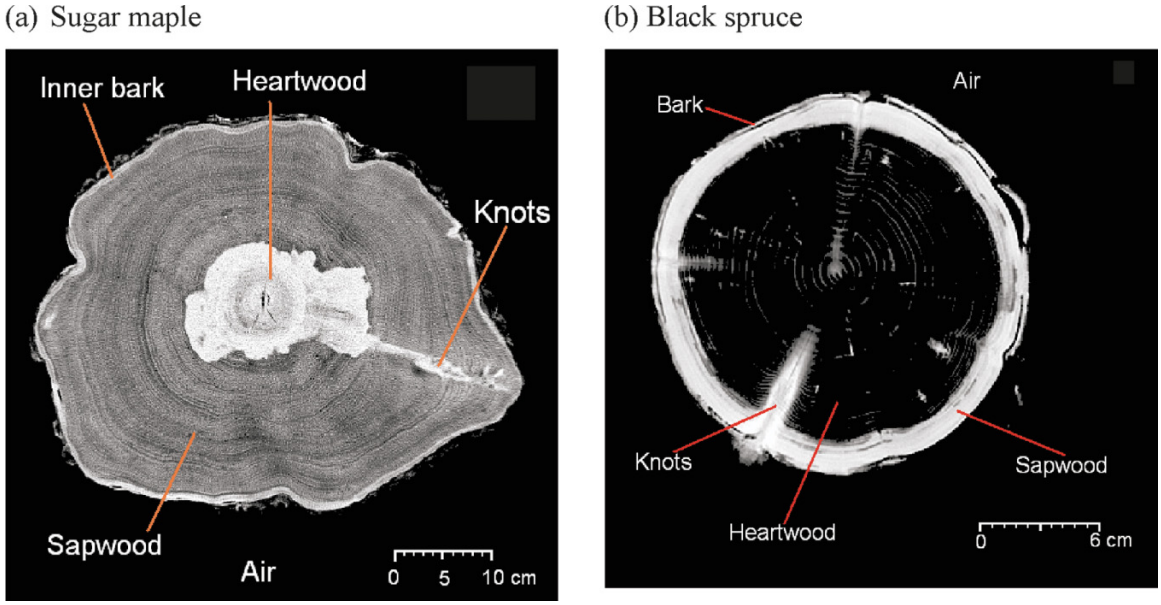

ble 3). For both the training and the validation data sets, better classification accuracy was achieved for sapwood in the case of sugar maple logs and for heartwood in the case of black spruce logs (Table 3). In the case of sugar maple logs, heartwood is difficult to distinguish from knots because of similar GL values (Wei et al. 2008*a*). In the case of black spruce logs, sapwood is difficult to distinguish because of a high spectral variability of the sapwood class and confusion with bark and knots, each of them being spectrally similar to sapwood (Wei et al. 2010). Wei et al. (2008*a*) suggested applying a median filter after classification for improving the visual appearance of the images, but this filter did not improve classification accuracies in the case of sugar maple logs (Rojas et al. 2006).

While the maximum likelihood classifier produces better classification accuracies than simple segmentation algorithms, the overall accuracy is still too low for an operational use. Also, the maximum likelihood classifier performance for detecting sapwood on CT images acquired over sugar maple logs was shown to be limited to log moisture content ranging from 44% to 67% (Rojas et al. 2007).

Other image classification techniques have been investigated to identify heartwood and sapwood in CT images. One of the widely used image processing techniques is the artificial neural network (ANN). Among all the ANN types, the feed-forward back-propagation (BP) ANN is one of the most easy to use and is effective for solving pattern-matching problems (Schmoldt et al. 2000*a*). In studies aiming to detect defects, BP-ANNs have been developed for various hardwood species, but the classification of heartwood and sapwood over CT slices was tested only for yellow-poplar (*Liriodendron tulipifera* L.), which was the only hardwood species for which sapwood was visible on CT slices (Schmoldt et al. 2000*a*). The CT slices were fist preprocessed to remove the air background and internal voids and to normalize the GL histograms to accommodate different hardwood species. The BP-ANN classifier was trained using GL values from the neighbourhood of the pixel to be classified. It then classified each pixel to a particular labeled class. Both studies considered a 3D neighbourhood, while Schmoldt et al. (2000*a*) also considered a 2D neighbourhood. Schmoldt et al. (2000*a*) also used the distance from the pith as input in the ANN classifier. Morphological post-processing was then used to remove spurious misclassifications and refine the shapes of detected image regions. The ANN classifier was able to achieve an overall classification accuracy higher than 95% (Table 4), but no specific sapwood and heartwood class accuracy was provided (Schmoldt et al. 2000*a*). The 2D classifier worked better for the single species, but the 3D classifier was better as multispecies classifier (Table 4). For both 2D and 3D classifiers, the single-species classifiers gave better classification accuracies than the multispecies classifiers (Table 4).

An improved version of BP-ANN was used to identify heartwood and sapwood over CT slices acquired over sugar maple logs (Wei et al. 2008*b*) and black spruce logs (Wei et al. 2008*b*, 2009*a*). First, in contrast with Schmoldt et al.'s studies, the BP-ANN was trained not only with spectral information (GL values) and distance information but also using the same seven textural features as for the maximum likelihood classifier (Wei et al. 2008*a*, 2010). Second, Wei et al. (2008*b*, 2009*a*) used the resilient BP training algorithm (Riedmiller and Braun 1993) instead of the commonly used steepest gradient descent with momentum algorithm (Freeman and Skapura 1991). The resilient BP training algorithm was shown to be five to six times faster for converging (Riedmiller and Braun 1993; Wei et al. 2008*b*). The classification accuracies obtained for the heartwood and sapwood with the BP-ANN classifier (Table 4) were significantly higher compared with the accuracies obtained with the maximum likelihood classifier (Table 3), reaching even a classification accuracy of 100% in some cases (Table 4). As expected, the classification accuracies are lower when the algorithms are validated on other images than those used for their training (Table 4).

Table 3. Producer's overall and class accuracy (as defined by Congalton (1991)) for identifying log features over CT slices using the maximum likelihood classifier.

Species	Data set	Log type	Sapwood	Heartwood	Rot	Splits	Knots	Bark	Overall	Reference(s)
Sugar maple (*Acer saccharum* Marsh.)	Training	Green log	98.6	46.3	54.2	75.0	64.8	22.6	83.1	Rojas et al. 2006
		Wood yard	81.8	78.8	10.5	0.0	44.7	na	78.0	Rojas et al. 2006
			85.6	71.3			72.1	83.0	79.8	Wei et al. 2008*a*
	Validation		75.8	60.0			73.4	80.5	72.2	Wei et al. 2008*a*
Black spruce (*Picea mariana* (Mill.) BSP)	Training		73.0	87.5			78.3	81.6	80.9	Wei et al. 2009*a*, 2010
	Validation		60.9	83.0			67.6	53.2	71.0	Wei et al. 2010

Table 4. Overall and class accuracy for identifying log features over CT slices using a BP-ANN classifier.

					Overall (%)		
Species	Sapwood	Heartwood	Knots	Bark	2D	3D	Reference
Red oak (*Quercus rubra* L.) and water oak (*Quercus nigra* L.)						95.0	Li et al. 1996
Red oak						90.0	Schmoldt et al. 1996
Red oak					96.0	95.0	Schmoldt et al. 2000*a*
Black cherry (*Prunus serotina* Ehrh.)					97.0	97.0	
Yellow-poplar (*Liriodendron tulipifera* L.)					96.0	94.0	
Red oak and black cherry					96.0	97.0	
Yellow-poplar and black cherry					90.5	92.0	
Red oak and yellow-poplar					94.0	95.0	
Red oak, yellow-poplar, and black cherry					93.0	93.0	
Scots pine (*Pinus sylvestris* L.)					95.9		Nordmark 2002
Sugar maple (*Acer saccharum* Marsh.)							Wei et al. 2008*b*
Training logs	100.0	99.3	97.9	96.7	98.5		
Validation logs	98.4	100.0	75.2	84.6	89.5		
Black spruce (*Picea mariana* (Mill.) BSP)							
Training logs	98.1	100.0	95.5	96.8	97.6		Wei et al. 2009*a*
Validation logs	80.7	99.7	91.8	97.6	92.4		Wei et al. 2008*b*

Note: The CT images were acquired over drying logs.

Knots

One important log defect to be identified in logs is the knots; hence, identifying knots is the purpose of most of CT studies applied to log feature identification. The knot is either a dormant bud or the portion of a branch that is embedded in the wood of a tree trunk. In a longitudinally sawn plank, a knot will appear as a roughly circular or elliptical feature where the grain direction of the wood is up to 90° different from the grain direction of the surrounding part of the wood.

Because optimization of log breakdown should take into account the location of knots, knottiness is a good timber quality indicator. Knot parameters extracted from CT images have been shown to be influenced by several tree or stand variables, such as spacing and thinning regimes, class of diameter at breast height, and position in the tree stem in the case of Scots pine (Moberg 1999). Knot size and orientation parameters have been correlated with tree, stand, and site variables in the case of Scots pine (Björklund and Petersson 1999; Moberg 2006) and in the case of Norway spruce (Moberg 2006). All of the knot inventory data relationships were later used to predict lumber volume and grade recovery in sawmill simulations (e.g., Moberg and Nordmark 2006).

On CT images, knots appear typically with a lighter tone (higher GL values) than the surrounding area because they are made of high-density cells. These differences in GL values among log features allow the development of segmentation algorithms that use GL value histogram thresholds to identify potential defect regions on CT images (Taylor et al. 1984; Funt and Bryant 1987; Grundberg and Grönlund 1991, 1992; Wells et al. 1991; Schmoldt et al. 1993; Som et al. 1993, 1995; Hagman and Grundberg 1995; Zhu et al. 1996; Oja 1997, 2000; Bhandarkar et al. 1999; Jaeger et al. 1999; Aguilera et al. 2002; Andreu and Rinnhofer 2003; Longuetaud et al. 2005). The labeling of the identified areas is done using various techniques. Knots are labeled based on their typical elliptical shape (Taylor et al. 1984; Funt and Bryant 1987). Wells et al. (1991) used principal components analysis, nonlinear combination of GL statistics vectors (mean, variance), and mathematical morphology operations to identify knots. Grundberg and Grönlund (1991) labeled, as sound knots, every image area having a GL higher than 1100 $kg \cdot m^{-3}$ in the case of Scots pine logs. For the same species, Grundberg and Grönlund (1991, 1992) proposed the following image processing method. First, a low-pass filter is used to

Can. J. For. Res. Downloaded from www.nrcresearchpress.com by UNIVERSITETSBIBLIOTEKET I TRONDHEIM on 09/18/12
For personal use only.

Table 5. Knot detection accuracy as a function of the species and the knot diameter class using thresholding segmentation algorithms.

Species	Knot diameter class (mm)	Accuracy (%) 2D analysis	3D analysis	Reference
Norway spruce (*Picea abies* (L.) Karst.)	≥7	94		Oja 2000
	≥10	90		Oja 1997
	<10	42		
Radiata pine (*Pinus radiata* D. Don)	≥10	100.0–162.5[a]	50.0–87.5	Aguilera et al. 2002
	<10	66.7–112.5[a]	18.4–46.7	
Sugar maple (*Acer saccharum* Marsh.)		84	81.4	Bhandarkar et al. 1999
White ash (*Fraxinus americana* L.)		90.2	89.3	
Red oak (*Quercus rubra* L.)		83.2	80.8	
Black walnut (*Juglans nigra* L.)		85.7	83.3	
Scots pine (*Pinus sylvestris* L.)		84		Nordmark 2003
Scots pine (*Pinus sylvestris* L.)		~100[b]		Longuetaud et al. 2005

[a]The destructive method does not identify properly some knots.

[b]They were not able to differentiate between the actual annual growth unit whorls and the lammas shoots.

Can. J. For. Res. Downloaded from www.nrcresearchpress.com by UNIVERSITETSBIBLIOTEKET I TRONDHEIM on 09/18/12
For personal use only.

smooth the growth rings from the CT images. Then 10 concentric surfaces (five in the sapwood and five in the heartwood) around the pith are delineated and processed. Knots are identified only on the heartwood concentric surfaces based on a fixed GL threshold of 875. The algorithm then computed 11 parameters (like diameter, angle, distance from the pith, etc.) for the knots in the heartwood. The parameters are used to fit knot geometrical models. These help in finding knots in the sapwood that has similar spectral responses as the knots. While the location of the knots is relatively good, knot geometrical parameters are overestimated. Grundberg and Grönlund's (1991, 1992) method was validated on CT images acquired over Norway spruce logs (Oja 1997). An improved version of the image processing method, which better detects small knots and positions the knots in the longitudinal direction, was validated over Norway spruce logs (Oja 2000) and over radiata pine logs (Aguilera et al. 2002). Elsewhere, knots have been labeled using first edge detection algorithms and then a 3 × 3 mask adapted to the knot radial structure (Som et al. 1993) or as being the disturbing elements of the growth rings that were detected through mathematical morphology operations (Som et al. 1995).

In some of the previous listed studies, defect identification and labeling are helped with the use of 3D information. Concentric surfaces from successive CT slices helped to identify the branches in 3D (Grundberg and Grönlund 1992). Knots were labeled using segmentation of images based on subtracted successive CT slices (Som et al. 1993; Jaeger et al. 1999). Correlation analysis across corresponding defect-like regions in neighbouring CT slices was used to verify whether the region, previously identified as a potential defect region, is indeed a defect-free or not region (Bhandarkar et al. 1999). A heuristic rule based recognition algorithm that is based on threshold values of 3D volume descriptors was used to detect defects on red oak (*Quercus rubra* L.) and yellow-poplar logs (Schmoldt et al. 1993). 3D intensity-related and orientation-related characteristics of log defects were used to label the segmented images into specific typical zones using a knowledge-based method called the Dempster–Shafer theory of evidential reasoning (Zhu et al. 1996). The longitudinal GL profile of the log was extracted from stacks of CT slices to locate knots lengthwise (Flood et al. 2003; Longuetaud et al. 2005).

The knot detection accuracy that was achieved by these segmentation algorithms depends on the species and knot diameter (Table 5). However, these algorithms also have several limitations. The algorithms rely heavily on thresholds that are sometimes difficult to determine. For example, in most of the studies, the developed methods were applied only to green logs, which are characterized by large differences in density caused by the difference in moisture content, and to knots, which are located in the heartwood area, because sapwood and knots have the same density (Grundberg and Grönlund 1991, 1992; Wells et al. 1991; Hagman and Grundberg 1995; Longuetaud et al. 2005). Also, the segmentation algorithms do not work properly for young trees for which heartwood has a too small area (Nordmark 2002). In other studies, moisture content variation within the green log was identified as a source of error in distinguishing defects from sound wood because the difference in CT numbers is attributed to the difference in moisture content rather than to that in density (Taylor et al. 1984; Funt and Bryant 1987; Schmoldt et al. 1993; Schad et al. 1996; Müller and Teischinger 2001; Bucur 2003*a*; Middleton et al. 2003; Alkan et al. 2007; Longuetaud et al. 2007; Brüchert et al. 2008). The algorithms that labeled the identified regions based on a supposed elliptical shape of knots did not work very well for identifying knots with irregular shapes on CT slices (Bhandarkar et al. 1999). Finally, in all of these studies, the segmentation and region labeling were done in two steps and thus the computing time of the algorithms was increased.

Similar to the identification of heartwood and sapwood, image segmentation and labeling for knots can be done in one step using Bayesian maximum likelihood classifiers. Using the same maximum likelihood classifier as for the identification of heartwood and sapwood, knots were identified in CT images acquired over sugar maple logs (Rojas et al. 2006, 2007; Wei et al. 2008*a*) and over black spruce logs (Wei et al. 2009*a*, 2010). The resulting producer's accuracies for knot detection in both Rojas et al.'s and Wei et al.'s studies

Can. J. For. Res. Downloaded from www.nrcresearchpress.com by UNIVERSITETSBIBLIOTEKET I TRONDHEIM on 09/18/12
For personal use only.

are presented in Table 3. Table 3 results show that Wei et al.'s algorithm, which considers also the textural image information, gave better knot detection over sugar maple logs than Rojas et al.'s algorithm, which is based only on the spectral image information. For Rojas et al.'s algorithm, the classification was better for freshly cut logs than for logs that dried sometimes on the wood yard. As expected, applying the maximum likelihood classifier to validation CT slices, i.e., those that were not used for training the classifier, reduced the class accuracies for both species but mainly for the black spruce logs (Table 3). The rather modest classification accuracy of knots in sugar maple logs can be explained because of confusion with heartwood that has similar GL values as knots (Wei et al. 2008*a*). In the case of black spruce logs, knots are spectrally similar to sapwood and inner bark (Wei et al. 2010). Similar to the heartwood and sapwood classification accuracies, the knot classification accuracy obtained by the maximum likelihood classification is too low for operational use of the method in processing CT images of logs.

Other more sophisticated algorithms were proposed. For hardwood (white ash (*Fraxinus americana* L.), sugar maple, and red oak) logs, Bhandarkar et al. (2006) used a dynamic contour extraction technique based on Kalman Snakes to reconstruct the knots and the outer boundary of the log in 3D space. They achieved a detection accuracy of 100% for all the species. The BP-ANN algorithms that were developed for the identification of heartwood and sapwood ("Heartwood and sapwood" section above) were used to detect defects over CT images acquired over red oak and water oak (*Quercus nigra* L.) logs (Li et al. 1996; Schmoldt et al. 1996, 1999, 2000*a*; Sarigul et al. 2003), yellow-poplar and black cherry (*Prunus serotina* Ehrh.) logs (Schmoldt et al. 1999, 2000*a*), sugar maple logs (Wei et al. 2008*b*), black spruce logs (Wei et al. 2009*a*), and Scots pine logs from young stands (Nordmark 2002). For these logs, Nordmark (2003) computed from the classified images the same 11 knot geometrical parameters as those of Grundberg and Grönlund's method.

Similar to the heartwood and sapwood classification accuracies, the BP-ANN classifiers for knot detection produced overall classification accuracy above than 90% (and often higher than 95%) (Table 4), which is higher than those produced by the maximum likelihood classifier (Table 3). The low classification accuracies occurred when using validation logs or with multispecies classifiers (Table 4). Only Wei et al. (2008*b*, 2009*a*) computed classification accuracy for the knot class, which ranges from 75.2% to 97.9%, depending on the tested species and the type of data sets (Table 4). The post-classification morphological method of Sarigul et al. (2003) further improved the labeling accuracy by 4.6%–6% while at the same time allowed the removal of many spurious regions from the interior of the wood and many incorrect defect regions from the outside edge of the wood. The method also allows the production of more rounded shapes of image regions and an enhanced representation for the splits. The BP-ANN classifier was also shown to be 22 times faster than knowledge-based classification methods (Schmoldt et al. 1996, 2000*a*) and to be more suitable for young trees with lower heartwood area (Nordmark 2002, 2003). However, BP-ANN classifiers that only use GL values as inputs were reported to have problems distinguishing between knots and moisture pockets, both being characterized by high GL values in the CT images. BP-ANN classifiers were also developed to classify knots into three categories, which differ according to the knot biological status (living, dead, or rotten), with an accuracy ranging between 85% and 93%. The knots were classified over CT images using Grundberg and Grönlund's segmentation method (Hagman and Grundberg 1995).

Other defects

Among all other defects occurring in logs, decay is one of the most current. It can appear as very dark zones because of very low GL values. These values can be sometimes close to the image background (air) (Schmoldt et al. 1996), particularly when they are related to air pockets, such as those produced by advanced decay (Benson-Cooper et al. 1982). However, on CT images, some decay can have a similar appearance to healthy wood (Rinnhofer et al. 2003). When fungal decay binds moisture, the GL values can be high because of the increase in local density (Habermehl and Ridder 1995).

Besides portable gamma-ray CT images (Habermehl and Ridder 1995; Niemz et al. 1998), X-ray CT images have been tested for decay detection in logs (e.g., Benson-Cooper et al. 1982; Petutschnigg et al. 2002; Rinnhofer et al. 2003; Rojas et al. 2005, 2006) and in other wood products, such as historical wood specimens (Bahýl and Rohanová 2006). However, Petutschnigg et al. (2002) was not able to detect rot in Norway spruce logs using CT images, unless they added log moisture content in the regression analysis. The resulting identification accuracy was 80%. Yu and Qi (2008) showed that a method based on multifractal theory was better than classical methods for edge detection in CT images acquired over logs that were subjected to decay.

Other defects that can affect logs are due to insect attacks. Benson-Cooper et al. (1982) showed that insect tunnels that were filled with air appear dark on CT images acquired over Tasmanian blackwood (*Acacia melanoxylon* R. Br.) and red beech (*Nothofagus fusca* (Hook. f.) Oerst.) logs. Kozakiewicz and Gawarecki (2003) were able to detect insect tunnels bored by *Anobium punctatum* De Geer in an 18th century wooden angel sculpture using CT images.

Resin pockets are another defect common in softwoods and can cause economical losses due to rejection of specimens during assembling or coating processes. They appear as small lenses of resin lying along the annual rings of trees (Temnerud and Oja 1998). In slash pine, they are always associated with the existence of wood tissue fracture or shake (Harding et al. 2007). Resin pockets are usually smaller than knots. In Norway spruce, the size of resin pockets varies from a minimum length, width, and thickness of 3.0, 2.5, and 0.5 mm to a maximum of 175, 65, and 7 mm, respectively (Temnerud 1997). According to Oja and Temnerud (1999) and Harding et al. (2007), the high density of resin gives a contrast between resin pockets and normal heartwood over green log CT images. Resin pockets can usually be distinguished from knots (that also show high GL values) because both have a completely different geometrical shape, at least if they are large enough. While green sapwood has similar density to resin pockets, resin pockets can still be identified in green sapwood because of a thin area with low density surrounding the pocket. Resin pocket detection was

Can. J. For. Res. Downloaded from www.nrcresearchpress.com by UNIVERSITETSBIBLIOTEKET I TRONDHEIM on 09/18/12
For personal use only.

done using 3D log information through stereology analysis applied to CT images acquired over Norway spruce logs (Temnerud and Oja 1998) or through volume rendering applied to CT images acquired over slash pine logs (Harding et al. 2007). The volume of resin pockets was estimated with a coefficient of error of less than 10% by Temnerud and Oja (1998). While large resin pockets were easy to detect, detection of small resin pockets was most difficult because it requires differentiation from compression wood (Temnerud and Oja 1998) or because of confusion with knots or local dry areas (Oja and Temnerud 1999).

The last type of internal log defect is related to the type of wood. For sugar mapl, the heartwood is coloured and should be considered as a defect (Rojas et al. 2006). Coloured heartwood was easily identified on CT images using the maximum likelihood classifier (Table 3) (Rojas et al. 2006; Wei et al. 2008*a*) or BP-ANN classifier (Wei et al. 2008*b*), but some confusion occurred with knots (Wei et al. 2008*a*). European beech has a red heart that should be detectable on CT images because it corresponds to a low moisture content area (Bauch and Koch 2001). However, red heart often appears on old trees that have a too large diameter to be scanned with medical scanners. Pruned radiata pine logs often experience a defective core that is a central area of the stem that is produced by the removal (pruning) of dead or living branches to produce knot-free wood. Defective cores can be identified on CT images (Benson-Cooper et al. 1982; Rojas and Ortiz 2009). Indeed, a defective core has heterogeneous GL values because it is constituted of oval light areas (corresponding to knots) within a dark zone, which constitutes the rest of the defective core. Rojas and Ortiz (2009) used a maximum supervised classifier to classify CT images into three classes (knots, defect-free zone, and defective core) and applied a 7×7 median filter on the classified images. They achieved an overall classification accuracy of 92.7% and a class accuracy for the defective core of 98.5%.

Reaction wood is another important defect in wood that occurs very frequently in some wood raw material. It appears as lighter areas contrasting with opposite wood. Marčok et al. (1996) showed that reaction wood can easily be identified on CT images acquired over European beech logs with moisture content above the fibre saturation point because zones with reaction wood have on average a higher moisture content than the opposite wood.

3D reconstructions

Most previous studies are limited to 2D image analysis, which does not make full use of the 3D nature (voxel) of CT images. 3D internal information of the full-length log is used, for example, in sawing optimization programs such as the GRAphic Sawing Program (GRASP) (Occeña and Schmoldt 1996), TOPSAW (Guddanti and Chang 1998), virtual SawMill (vSM) (Chiorescu and Grönlund 2000), the computer vision-based lumber production planning system (CVLPPS) (Bhandarkar et al. 2006), and OPTITEK from FPInnvations (Grondin and Drouin 1998). 3D reconstruction of the full-length log is therefore needed, as CT scanning is often performed over log sections, particularly if medical scanners are used. While some studies directly acquired 3D cone-beam tomography images (Flood et al. 2003; Seger and Danielsson 2003), all of the other studies reconstructed 3D images of logs from successive 2D CT images using various techniques.

Several studies used volume rendering techniques to visualize volumetric data. Volume rendering techniques render the opacity and colour of the voxel of the whole volume data using a red–green–blue–alpha value that depends on the original signal intensity from the CT slice. There are two main types of volume rendering techniques (Meißner et al. 2000). The first one is indirect volume rendering. It first converts the volumetric data into a set of polygonal isosurfaces and then renders with polygon rendering hardware. A common indirect volume rendering method for extracting isosurfaces from volume data is the Marching Cubes algorithm (Lorensen and Cline 1987). The algorithm proceeds through the scalar field, taking eight neighbour locations at a time (thus forming an imaginary cube) and then determining the polygon(s) needed to represent the part of the isosurface that passes through this cube. The individual polygons are then fused into the desired surface. The algorithm has been implemented into open-source 3D visualization software such Slicer 3.4 (www.slicer.org/) (Gering et al. 2001).

The second type of volume rendering is a direct volume rendering that directly renders the volumetric data without the intermediate conversion step. It is a computationally intensive task that may be performed using several approaches, including raycasting (Levoy 1988), splatting (Westover 1990), shear-warp (Lacroute and Levoy 1994), and 3D texture-mapping hardware (Cabral et al. 1994). Meißner et al. (2000) showed that the best direct volume rendering methods are the 3D texture-mapping hardware and shear-warp. Raycasting approaches have been implemented in open-source software such as ImageVis3D (www.sci.utah.edu/cibc/software/41-imagevis3d.html) and Voreen (Meyer-Spradow et al. 2009) and in commercial software such as VoluMedic (www.volumedic.com/). Open-source software Volpack (www.ostatic.com/volpack/) uses the shear-wrap method, whereas Volview (www.kitware.com/) is based on the 3D texture-mapping hardware method (Constantinescu and Vlădoiu 2009). Direct volume rendering methods should be more efficient than indirect volume rendering methods because the complexity of the extracted polygonal mesh can overwhelm the capabilities of the polygon subsystem, especially when the object is complex or large or when the isosurface is interactively varied (Meißner et al. 2000).

All of these algorithms have been developed mainly for medical applications, but some have been tested for log or board 3D visualization. The Marching Cubes algorithm was used to visualize internal defects in 3D white spruce (*Picea glauca* (Moench) Voss) logs and sawn logs (Middleton et al. 2003), to reconstruct termite (*Cryptotermes secundus* Hill) gallery systems in dead radiata pine logs (Fuchs et al. 2004), to assess 3D wet-wood distributions in heartwood of subalpine fir logs (Alkan et al. 2007), and to identify internal features (bark, sapwood, heartwood, and knots) in 3D in the case of sugar maple and black spruce logs (Wei et al. 2009*b*). With Volview, Aguilera et al. (2002) reconstructed 3D log CT images to detect knots in radiata pine logs. Bhandarkar et al. (1999) used a modified version of the z-buffer algorithm that simultaneously renders 3D opaque and semi-transparent objects (Foley et al. 1990) to detect and locate defects in CT images acquired over white ash, red oak, sugar

Can. J. For. Res. Downloaded from www.nrcresearchpress.com by UNIVERSITETSBIBLIOTEKET I TRONDHEIM on 09/18/12
For personal use only.

maple, and black walnut logs. Both Aguilera et al. (2002) and Bhandarkar et al. (1999) achieved a knot detection accuracy that was lower than those produced using 2D CT images (Table 5). Volume rendering software was also used to reconstruct 3D resin pockets and knot whorls from CT images acquired over slash pine logs (Harding et al. 2007).

Whatever method is used for obtaining 3D reconstruction, interpolation techniques can be applied to estimate CT values between the measured CT slices to reduce the number of CT slices needed for a satisfactory reconstruction of the object. Xu et al. (2005) used cubic natural spline interpolation functions to reconstruct European ash (*Fraxinius excelsior* L.) logs, while zu Castell et al. (2005) used radial basis interpolation functions to reconstruct Norway spruce logs. Radial basis interpolation functions have the advantage of taking into account that log structures differ more in the radial than in the longitudinal direction; hence, better interpolation results for log structures are obtained.

Currently, log 3D information for sawing optimization programs is mainly external and derived from laser measurements. There are several issues with operational use of CT images in 3D reconstruction of logs. These are related first to lower accuracy in internal feature identification than produced using 2D CT images (Table 5). Another limitation is related to the high computation time required that is not yet suitable in online systems. Wei et al. (2009*b*) showed that reconstruction of a 3D image from 72 thick CT slices, each of them having 10 mm thickness, requires between 15 and 20 min to complete over a desktop computer with Pentium (R) 4CPU 2.4 GHz processing speed.

Operability of X-ray CT scanners in real wood industry environments

Since 1972, CT scanners have been used as medical diagnosis tools (Cormack 1963; Hounsfield 1980). As described above, they have been used widely for laboratory testing because of the similar organic nature of wood and the human body. However, they are not suitable for real wood industry environments. First, their scanning speed is usually not compatible with the production flow rate. For example, Oja (1997) reported that it took about 2.5 h to scan one Norway spruce log every 10 mm with a 5 mm wide X-ray beam with a medical CT scanner (Siemens SOMATOM ART). They were able to achieve a knot identification accuracy of 90%. However, Wagner et al. (1989) tested a medical CT scanner (Imatron C-100) in its ultrafast configuration that was able to acquire 34 images per second over a water oak log. Such a scanning speed approaches those required to be used in commercial sawmills and veneer plants. The CT scanner in its ultrafast mode can scan logs having a maximum diameter of 38.1 cm. While all log defects can be seen on CT images, Wagner et al. (1989) did not quantitatively test the image quality with respect to log feature identification accuracies.

The speed of a CT scanner is strongly related to the resolution along the feeding direction. Increasing CT scanning speed can be done using either a low radiometric image resolution or a low spatial image resolution. Reduced radiometric resolution can affect the ability to distinguish different density areas in logs, which is the basis of any CT image use in the wood industry (Schad et al. 1996). Spatial image resolution depends on pixel size, scan thickness, and scan frequency. Scanning speed is more dependent on longitudinal scanning rates (thickness and frequency) than within-slice resolution (pixel size). For hardwood logs, Thawornwong et al. (2003) did not observe any significant changes in the simulated lumber value yields when the spatial resolution of CT scans was reduced by doubling the pixel size, scan thickness, and scan frequency. However, detection of small or thin defects (i.e., metallic inclusions, cracks, and resin pockets) or defects that need the detection of annual rings (i.e., spiral grain) requires high spatial resolution CT images (Rinnhofer et al. 2003; Harding et al. 2007).

Second, even if CT scanning can be done with an appropriate speed, there is the need to have image processing algorithms that should be fast enough to be compatible with the production flow rate. Indeed, medical CT images are visually inspected offline by the radiologist for medical diagnosis purposes. In contrast, in the wood industry, image processing algorithms should allow automatic detection of the appropriate features, such as defects, for online production optimization. It should also be fast enough to be compatible with the production flow rate. Indeed, a CT scan of a single log usually produces a large amount of data to be processed. According to Benson-Cooper et al. (1982), a scan time of about 2 s allows the acquisition of some 400 000 data points. A CT scan of a single log can produce over several hundred megabytes of data (Li et al. 1996; Schmoldt et al. 1999; Rinnhofer et al. 2003). Grundberg and Grönlund (1991) proposed three methods for reducing the amount of data to be processed. The first method reduces the radiometric resolution of the image, for example from a 256 GL image to a 5 GL image. Such reduction is done through segmentation of the CT image using density threshold values. Such a decrease in radiometric resolution can lead to a lower ability to distinguish log features for which the density difference is too small (Schad et al. 1996). The second method reduces the spatial resolution of the CT image by increasing the pixel size from 0.5 to 5 mm, for example. Low spatial image resolutions have no discernable effect on lumber value yields (Thawornwong et al. 2003) but do have an effect on the detection of small or thin defects or annual rings (Rinnhofer et al. 2003; Harding et al. 2007). The third method processes only a portion of the CT image by searching knots only on 10 concentric surfaces around the pith. Knot geometrical models are derived from the heartwood knots and used to help find the sapwood knots that have a low spectral discrimination with the surrounding wood. Schmoldt et al. (1999) proposed the geometric data reduction model to eliminate slice data (in a recursive fashion) that do not exhibit unique centroidal displacement or size characteristics within a threshold value.

Another way of increasing image processing speed is to use more efficient image processing algorithms. One of the fastest ones that also produce high classification accuracies is the BP-ANN classifier. BP-ANN classifiers were able to process one image in 25 s (Li et al. 1996; Schmoldt et al. 1996), i.e., 22 times faster than a knowledge-based classifier (9 min) (Schmoldt et al. 1996). These BP-ANN classifiers should be 8–10 times faster on high-performance hardware (Schmoldt et al. 1996) and five to six times faster if a resilient BP algorithm is used (Riedmiller and Braun 1993; Wei

Can. J. For. Res. Downloaded from www.nrcresearchpress.com by UNIVERSITETSBIBLIOTEKET I TRONDHEIM on 09/18/12
For personal use only.

et al. 2008*b*). However, even with BP-ANN algorithms, the data amount should be reduced (Schmoldt et al. 1999).

Third, besides the difference in spatial resolution, radiometric resolution, and scanning speed, Schmoldt et al. (2000*b*) and Rinnhofer et al. (2003) listed several other technical differences between medical CT scanners and CT scanners suitable for the wood industry. The first one is the duty cycle, i.e., the frequency at which the CT scanner is used. Medical CT scanners are not used continuously, while CT scanners in a wood production line should be used 24 h a day 7 days per week. The second one is the reconstruction circle and the aperture size. Medical CT scanners have been designed with a maximum 40–50 cm reconstruction circle, which is too small for the diameter of the logs that should be processed. The third one is the environment in which CT scanners operate. Medical CT scanners are operated in a sanitized controlled hospital environment, whereas CT scanners in the wood industry would operate in harsh environments subjected to dust, temperature and humidity variations, typical of a sawmill or, even worse, outdoors in the wood yard. Other technical constraints that should be considered when operating an X-ray CT scanner in a wood plant include the usual radiation safety rules and the need for highly qualified service engineers to maintain the equipment (Benson-Cooper et al. 1982; Schad et al. 1996; Schmoldt et al. 2000*b*; Rinnhofer et al. 2003).

Other CT scanners that were tested over wood specimens have been developed for very dense metal objects, such as rocket engines and automobile scanning (Schad et al. 1996), and for luggage checking at airports (Schmoldt et al. 2000*b*, Rinnhofer et al. 2003). While airport scanner types are better than medical scanners with respect to their duty cycle, reconstruction circle, and their design for harsh environments (Schmoldt et al. 2000*b*; Rinnhofer et al. 2003; Harding et al. 2007), interpretation of the CT images is still done offline and the scanners do not have a suitable scanning speed. Also, airport scanners usually handle small objects (luggage) and would not be suitable for large objects (logs or lumber) (Schmoldt et al. 1999).

For all of these reasons, CT scanners that are specifically designed for the wood industry were developed. Schmoldt et al. (1999) designed an X-ray tangential CT scanner prototype for Omega International Inc. It claims to allow for time savings in the scanning process. First, the detector array and the fan beam are oriented to acquire data in the longitudinal log direction because the tangential CT scanner has the detector array parallel to the axis of rotation, while it is perpendicular in medical and airport CT scanners. Such a setup allows single continuous motion that collects the entire data set for all slices, while in medical and airport CT scanners, data for 180 views or 360 views are collected through several traverses that start and stop the linear motion each time. Second, it does not collect outside the object, while for medical and airport CT scanners, each detector can collect all rays through the entire object, including those through air (image background). The major drawback of this tangential scanner was the lack of a efficient image reconstruction algorithm.

Andreu and Rinnhofer (2001, 2003) and Rinnhofer et al. (2003) tested the Invision CTX 2500 scanner, an airport scanner that was adapted for log scanning. The Invision CTX 2500 scanner provides low spatial resolution images compared with classical medical scanners. Also, its scanning speed (1.5 $m \cdot min^{-1}$) is about 100 times too slow for volume-oriented high-speed sawmills. Flood et al. (2003) and Seger and Danielsson (2003) tested an X-ray linear cone-beam tomography device to directly obtain 3D images of logs that are translated at relatively high speed (2–3 $m \cdot s^{-1}$). The knots were reconstructed with sufficient accuracy to allow for quantitative optimization, but heartwood was barely distinguished from sapwood due to the missing data. In Canada, FPInnovations-Forintek has an industrial CT scanner that was designed by Bio-Imaging Research (Middleton et al. 2003; Alkan et al. 2007). Middleton et al. (2003) tested the scanner over white spruce logs. The images were processed to detect features such as pith, outer shape, and sapwood–heartwood boundary as well as to visualize log features (knots obscured by wet wood, wet pockets, knots, and cracks) and to reconstruct the 3D internal structure of the log. Image quality was not judged as being satisfactory enough to be included in a permanent CT stem bank database. Also, the image-processing algorithm that was used was developed for CT images acquired with a medical CT scanner. The scanner was used later on for detecting wet pockets and measuring moisture profile on subalpine fir boards (Alkan et al. 2007). In 2008, MiCROTEC GmbH announced the commercialization of an industrial CT scanner (CT.LOG) for log scanning (http://www.microtec.eu/), but its technical details appear to be commercially protected.

Besides the technical aspects, economical feasibility should also be analyzed because of the high cost of CT scanners (some cost figures are given in Benson-Cooper et al. (1982) and in Harding et al. (2007)). While most of the studies on the use of CT images have focussed on sophisticated automatic internal feature detection, very little work has been done on the economical viability of CT scanning in the wood industry (Harding et al. 2007). Some authors showed that lumber value gains can offset CT scanner costs (Hodges et al. 1990; Schmoldt et al. 2000*b*). According to Hodges et al. (1990), investments in CT scanning systems could be profitable with increases in lumber value yield of 5%–10% in the case of large hardwood sawmills (60–103 $m^3 \cdot year^{-1}$) and of 30% in the case of smaller hardwood sawmills (12–103 $m^3 \cdot year^{-1}$). However, it was suggested that the use of CT scanners is only economically sound for high-value logs (Schmoldt et al. 1993; Rinnhofer et al. 2003; Harding et al. 2007) and only on defect areas of logs (Schmoldt et al. 1993).

Alternatives to CT scanning

Because of the high cost of X-ray CT scanner equipments, other types of inexpensive sensors were investigated. One of these is electric resistivity tomography (ERT), which is originally a geophysical method that is based on the material electric resistivity or its reciprocal, electrical conductivity, both being related to object structure. ERT was applied to identify discoloured wood (Weihs 2001) and decay in trees (e.g., Bieker et al. 2010). However, according to Harding et al. (2007), the resulting ERT images are rather coarse in the case of logs and reliable results can only be achieved at a maximum depth of six or seven growth rings. Also, large changes in internal electrical conductivity can result in small voltage changes.

Can. J. For. Res. Downloaded from www.nrcresearchpress.com by UNIVERSITETSBIBLIOTEKET I TRONDHEIM on 09/18/12
For personal use only.

Microwave sensors have been tested over lumber for density and moisture content distribution (Bucur 2003*a*; Lundgren et al. 2006) and over logs (Kästner 2002; Harding et al. 2007), but additional research is needed, for example, to study the influence of the air gap between the microwave source and the log surface and the influence of log speed on measurement accuracy. Also, the large damping of the microwave signal creates a large noise in the signal and microwave sensors cannot be used on frozen logs. Such conditions often occur in wood yards in Canada.

Probably a multisensor approach should be used. Oja et al. (2004) reported an improvement in classification accuracy when classifying logs by centre board grade from 57% when using only 3D laser scanning to 66% when using both 3D laser and X-ray scanning of logs without knowledge about stem properties. Longuetaud et al. (2005) suggested that a combination of an X-ray CT scanner and an optical device would be the most appropriate to detect annual growth units over Scots pine logs because the annual GU whorls would be identified by the optical method, whereas lammas shoot whorls would be obtained by removing the optically detected whorls from the X-ray CT images. Hasenstab et al. (2006) compared the potential to detect cracks in woody building structures between ultrasound and X-rays and concluded that ultrasound is sensitive to cracks parallel to the surface and X-rays are sensitive to cracks perpendicularly aligned.

Conclusions

X-ray CT was proven as an internal board and log scanning technology. It has been utilized for wood density measurements, for wood moisture monitoring, and for internal log features that include pith, sapwood, heartwood, knots, and other defects. Annual growth ring measurements were more problematic to be detected on CT images because of the low spatial resolution of the images used. For log feature identification, our review shows that the BP-ANN was the most efficient CT image processing method. However, the method still requires calibration for each species or group of species and is therefore difficult to be generalized. Eventually, further work will be needed to test other image processing methods that also take into account the spatial dimensions of the image, such as fractal geometry and lacuranity analysis. In the reviewed literature, there were also some studies attempting to reconstruct 3D log or board images from 2D CT images. Most of them still needed to be validated by comparing against appropriate reconstructed reference 3D images (Jaeger et al. 1999; Wei et al. 2009*b*).

Medical scanners were shown to be inappropriate for the wood industry. Several industrial prototypes have been developed. There is now the need to validate most of the results that are presented in this study because they were mostly developed using medical CT scanners. Also, development of industrial CT scanners adapted for the wood industry requires further economical studies because of the high capital and operation costs associated with CT scanners as well as a thoughtful market analysis, as the wood industry is smaller than the medical sector. Because CT scanners are expensive, alternative inexpensive technologies have been tested such as ERT, microwave sensors, and the use of a multisensor approach. Each of them has its own advantages and disadvantages.

References

Aguilera, C., Ramos, M., and Salinas, D. 2002. Internal visualization of knots in radiata pine logs using X-rays. Maderas Cienc. Technol. **4**(2): 193–200.

Alkan, S., Zhang, Y.L., and Lam, F. 2007. Moisture distribution changes and wet-wood behavior in subalpine fir wood during drying using high X-ray energy industrial CT scanner. Drying Technol. **25**(3): 483–488. doi:10.1080/07373930601184023.

Andreu, J.-P., and Rinnhofer, A. 2001. Automatic detection of pith and annual rings on industrial computed tomography log images. *In* Proceedings of ScanTech, 9th International Conference on Scanning Technology and Process Optimization for the Wood Industry, Seattle, Washington. Wood Machining Institute, Berkeley, Calif. pp. 37–47.

Andreu, J.P., and Rinnhofer, A. 2003. Modeling knot geometry in Norway spruce from industrial CT images. *In* Proceedings of 13th Scandinavian Conference of Image Analysis (SCIA), Halmstad, Sweden, 29 June – 2 July 2003. *Edited by* J. Bigün and T. Gustavsson. Springer-Verlag, Berlin and Heidelberg. pp. 786-791.

Axelsson, B.O.M. 1994. Lateral cutting force during machining of wood due to momentary disturbances in the wood structure and degree of wear of the cutting tool. Eur. J. Wood Wood Prod. **52**(3): 198–204. doi:10.1007/BF02615223.

Bahýl, V., and Rohanová, A. 2006. The computer tomography internal wood structure recognition results. Ann. Warsaw Agric. Univ. For. Wood Technol. **58**: 20–23.

Bauch, J., and Koch, G. 2001. Biologische und chemische Untersuchungen über Holzverfärbungen der Rotbuche (*Fagus sylvatica* [L.]) und Möglichkeiten vorbeugender Maßnahmen. Bundesforschungsanstalt für Forst- und Holzwirtschaft, Universität Hamburg.

Benson-Cooper, D.M., Knowles, R.L., Thomson, F.J., and Cown, D. J. 1982. Computed tomographic scanning for the detection of defects within logs. New Zealand Forest Research Institute (FRI) Bull. No. 8.

Bhandarkar, S.M., Faust, T.D., and Tang, M. 1999. CATALOG: a system for detection and rendering of internal log defects using computer tomography. Mach. Vis. Appl. **11**(4): 171–190. doi:10.1007/s001380050100.

Bhandarkar, S.M., Luo, X., Daniels, R., and Tollner, E.W. 2006. A novel feature-based tracking approach to the detection, localization, and 3-D reconstruction of internal defects in hardwood logs using computer tomography. Pattern Anal. Appl. **9**(2–3): 155–175. doi:10.1007/s10044-006-0035-9.

Bieker, D., Kehr, R., Weber, G., and Rust, S. 2010. Non-destructive monitoring of early stages of white rot by *Trametes versicolor* in *Fraxinus excelsior*. Ann. For. Sci. **67**(2): 210p1–210p7. doi:10.1051/forest/2009103.

Björklund, L. 1999. Identifying heartwood-rich stands or stems of *Pinus sylvestris* by using inventory data. Silva Fenn. **33**(2): 119–129 Available from http://www.metla.fi/silvafennica/full/sf33/sf332119.pdf [accessed 31 May 2010].

Björklund, L., and Petersson, H. 1999. Predicting knot diameter of *Pinus sylvestris* in Sweden. Scand. J. For. Res. **14**(4): 376–384. doi:10.1080/02827589950152700.

Brashaw, B.K., Bucur, V., Divos, F., Gonçalves, R., Lu, J., Meder, R., Pellerin, R.F., Potter, S., Ross, R.J., Wang, X., and Tin, Y. 2009. Nondestructive testing and evaluation of wood: a worldwide research update. For. Prod. J. **59**(3): 7–14. Available from http://www.forestprod.org/FPJ59n3-feature.pdf [accessed 31 May 2010].

Can. J. For. Res. Downloaded from www.nrcresearchpress.com by UNIVERSITETSBIBLIOTEKET I TRONDHEIM on 09/18/12
For personal use only.

Brüchert, F., Baumgartner, R., and Sauter, U.H. 2008. Ring width detection for industrial purposes — use of CT and discrete scanning technology on fresh roundwood. *In* Proceedings of the Conference COST ACTION E53, Delft, The Netherlands, 29–30 October 2008. pp. 157–163. Available from http://www.coste53.net/downloads/Delft/Presentations/COSTE53-Conference_Delft_-Bruechert_Baumgartner_Sauter.pdf.

Bucur, V. 2003*a*. Ionizing radiation computed tomography. *In* Nondestructive characterization and imaging of wood. Springer Series in Wood Science, Springer-Verlag, Berlin, Germany. pp. 13–73. ISBN3540438408.

Bucur, V. 2003*b*. Techniques for high resolution imaging of wood structure: a review. Meas. Sci. Technol. **14**(12): R91–R98. doi:10.1088/0957-0233/14/12/R01.

Cabral, B., Cam, N., and Foran, J. 1994. Accelerated volume rendering and tomographic reconstruction using texture mapping hardware. *In* Proceedings of the Symposium on Volume Visualization. Association for Computing Machinery, New York. pp. 91–98.

Chiorescu, S., and Grönlund, A. 2000. Validation of a CT-based simulator against a sawmill yield. For. Prod. J. **50**(6): 69–76.

Congalton, R. 1991. A review of assessing the accuracy of classifications of remotely sensed data. Remote Sens. Environ. **37**(1): 35–46. doi:10.1016/0034-4257(91)90048-B.

Constantinescu, Z., and Vlădoiu, M. 2009. Adaptive compression for remote visualization. Buletinul, Universităţii Petrol – Gaze din Ploieşti, Seria Matematică - Informatică – Fizică, LXI (2/2009). pp. 49–58. Available from http://bmif.unde.ro/docs/20092/7ZoranMonica2.pdf [accessed 31 May 2010].

Cormack, A.M. 1963. Representation of a function by its line integrals with some radiological applications. J. Appl. Phys. **34**(9): 2722–2727. doi:10.1063/1.1729798.

Danvind, J. 2002. Measuring strain and moisture content in a cross section of drying wood using Digital Speckle Photography and Computerised X-ray tomography. *In* Proceedings of 13th International Symposium on Nondestructive Testing of Wood, Berkley, Calif., 19–21 August 2002. Forest Products Society, Madison, Wis.

Danvind, J., and Morén, T. 2004. Using X-ray CT-scanning for moisture and displacement measurements in knots and their surroundings. *In* Proceedings of the 5th COST ACTION E15: Advances in Drying of Wood, Athens, Greece, 22–24 April 2004. *Edited by* NAGREF/Forest Research Institute. Available from http://www1.uni-hamburg.de/cost/e15/papers/athens/24Danvind-Moren.pdf.

Davis, J., and Wells, P. 1992. Computer tomography measurements on wood. Industrial Metrology, **2**(3–4): 195–218. doi:10.1016/0921-5956(92)80004-D.

Du, C.G., Zhang, Q.S., Liu, Z.K., and Chen, S.G. 2009. Distribution characteristics of horizontal density of Chinese fir oriented laminated stick lumber (OLSL). J. Zhejiang For. College, **26**(4): 455–460.

Eriksson, J., Johansson, H., and Danvind, J. 2007. A mass transport model for drying wood under isothermal conditions. Drying Technol. **25**(3): 433–439. doi:10.1080/07373930601183785.

Fenyvesi, A., Béres, C., Raschi, A., Tognietti, R., Ridder, H.W., Molnár, T., Röfler, J., Lakatos, T., Csiha, I., and Paoletti, E. 1998. Sap-flow velocities and distribution of wet-wood in trunks of healthy and unhealthy *Quercus robur*, *Quercus petraea* and *Quercus cerris* oak trees in Hungary. Chemosphere, **36**(4–5): 931–936. doi:10.1016/S0045-6535(97)10150-3.

Flood, K., Danielsson, P.-E., and Seger, M.M. 2003. On 3D Segmentation of knots in 3D-volume data acquired from X-ray Linear cone-beam scanning. *In* Proceedings of the 5th International Conference on Image Processing and Scanning of Wood, Bad Waltersdorf, Austria, 23–26 March 2003. Joanneum Research Institute, Graz, Austria. pp. 151–160.

Foley, J., van Dam, A., Feiner, S., and Hughes, J. 1990. Computer graphics: principles and practice. 2nd ed. Addison-Wesley Publishing Company, Reading, Mass.

Freeman, J.A., and Skapura, D.M. 1991. Neural networks algorithms, applications and programming techniques. Addison-Wesley Publishing Company, Reading, Mass. pp. 93–101.

Freyburger, C., Longuetaud, F., Mothe, F., Constant, T., and Leban, J. M. 2009. Measuring wood density by means of X-ray computer tomography. Ann. For. Sci. **66**(8): 804p1804p9. doi:10.1051/forest/2009071.

Fromm, J.H., Sautter, I., Matthies, D., Kremer, J., Schumacher, P., and Ganter, C. 2001. Xylem water content and wood density in spruce and oak trees detected by high-resolution computed tomography. Plant Physiol. **127**(2): 416–425. doi:10.1104/pp.010194. PMID:11598217.

Fuchs, A., Schreyer, A., Feuerbach, S., and Korb, J. 2004. A new technique for termite monitoring using computer tomography and endoscopy. Int. J. Pest Manage. **50**(1): 63–66. doi:10.1080/0967087032000159300.

Funt, B.V., and Bryant, E.C. 1987. Detection of internal log defects by automatic interpretation of computer tomography images. For. Prod. J. **37**(1): 56–62.

Gering, D.T., Nabavi, A., Kikinis, R., Hata, N., O'Donnell, L.J., Grimson, W.E.L., Jolesz, F.A., Black, P.M., and Wells, W.M. , III. 2001. An integrated visualization system for surgical planning and guidance using image fusion and an open MR. J. Magn. Reson. Imaging, **13**(6): 967–975. doi:10.1002/jmri.1139. PMID:11382961.

Gierlik, E., and Dzbenski, W. 1996. Wood densitometry based on the radiometric methods. *In* Proceedings of the10th Symposium on Non-destructive Testing of Wood. *Edited by* Presses Polytechniques et Universitaires Romandes, Lausanne, Switzerland. pp. 217–225.

Grondin, F., and Drouin, N. 1998. Optitek sawmill simulator — user's guide. Forintek Canada Corporation, Québec, Qué.

Grönlund, A., Grundberg, S., Oja, J., and Nyström, J. 2005. Scanning techniques as tools for integration in the wood conversion chain — some industrial applications. Lignovisionen, **9**: 3–11.

Gruber, F. 1995. Hydraulische Architektur der Fichte: Splintermittlung und Splint-Nadelmasse Beziehungen. Allg. Forst Z. **50**(15): 807–808.

Grundberg, S., and Grönlund, A. 1991. Methods for reducing data when scanning for internal log defects. *In* Proceedings of the 4th International Conference on Scanning Technology in the Wood Industry, San Francisco, Calif. 28–29 October 1991. Luleå University of Technology, Luleå, Sweden.

Grundberg, S., and Grönlund, A. 1992. Log scanning - extraction of knot geometry. *In* Proceedings of the 1st International Seminar/Workshop on Scanning Technology and Image Processing on Wood, Skellefteå, Sweden. 30 August – 1 September 1992. Luleå University of Technology, Luleå, Sweden.

Guddanti, S., and Chang, S.J. 1998. Replicating sawmill sawing with TOPSAW using CT images of a full-length hardwood log. For. Prod. J. **48**(1): 72–75.

Habermehl, A., and Ridder, H.W. 1995. Computerised tomographic investigations of street and park trees. Arboricult. J. **19**(4): 419–437.

Hagman, P.O.G., and Grundberg, S.A. 1995. Classification of Scots pine (*Pinus sylvestris*) knots in density images from CT scanned logs. Eur. J. Wood Wood Prod. **53**(2): 75–81. doi:10.1007/BF02716393.

Can. J. For. Res. Downloaded from www.nrcresearchpress.com by UNIVERSITETSBIBLIOTEKET I TRONDHEIM on 09/18/12
For personal use only.

Hansson, L., and Antti, L. 2008. Modeling microwave heating and moisture redistribution in wood. Drying Technol. **26**(5): 552–559. doi:10.1080/07373930801944713.

Haralick, R.M., Shanmugam, K., and Dinstein, I. 1973. Texture characteristics for image classification. IEEE Trans. Syst. Man Cybern. **3**(6): 610–621. doi:10.1109/TSMC.1973.4309314.

Harding, K., Davis, J., Coopley, T., Selleck, A., and Haslett, T. 2007. Resin defect impacts on the value of graded recovery and evaluation of technologies for internal defect detection in slash pine logs. Tech. Rep. PN04.3005. Report to the Forest and Wood Products Research and Development Corporation, Melbourne, Australia.

Hasenstab, A., Osterloh, K., and Krause, M. 2006. Testing of wooden construction elements with ultrasonic echo technique and X-ray. *In* Proceedings of the 9th European Conference on Non-Destructive Testing, Berlin, Germany, 25–29 September 2006. pp. 1–8. Available from http://www.ndt.net/article/ecndt2006/doc/Th.2.4.1.pdf [accessed 31 May 2010].

Hattori, Y., and Kanagawa, Y. 1985. Non-destructive measurement of moisture distribution in wood with a medical X-ray CT-scanner. I. Accuracy and influencing factors. Mokuzai Gakkaishi, **31**: 974–982.

Hodges, D.G., Anderson, W.C., and McMillin, C.W. 1990. The economic potential of CT scanners for hardwood sawmills. For. Prod. J. **40**(3): 65–69.

Hou, Z.Q., Wei, Q., and Zhang, S.Y. 2009. Predicting density of green logs using the computed tomography technique. For. Prod. J. **59**(5): 53–57.

Hough, P.V.C. 1962. Method and means for recognizing complex patterns. U.S. Patent 3,069,654, 18 December 1962. U.S Patent and Trademark Office, Alexandria, Va.

Hounsfield, G.N. 1980. Computed medical imaging. Science, **210** (4465): 22–28. doi:10.1126/science.6997993. PMID:6997993.

Jaeger, M., Leban, J.-M., Borianne, P., Chemouny, S., and Saint André, L. 1999. 3D stem reconstruction from CT scan exams. From log external shape to internal structures. *In* Proceedings of the 3rd IUFRO Workshop "Connection between Silviculture and Wood Quality through Modelling Approaches and Simulation Software", IUFRO Working Party S5.01-04 "Biological Improvement of Wood Properties" and Équipe de Recherches sur la Qualité des Bois, INRA-Nancy, La Londe-Les-Maures (France), 5–12 September 1999. *Edited by* G. Nepveu. INRA, Nancy, France. pp. 399–409.

Johansson, J., and Kifetew, G. 2010. CT-scanning and modelling of the capillary water uptake in aspen, oak and pine. Eur. J. Wood Wood Prod. **68**(1): 77–85. doi:10.1007/s00107-009-0359-4.

Kästner, A. 2002. Non-invasive multidimensional imaging applied on biological substances. Ph.D. thesis, Technical Report No. 428, Department of Signals and Systems, Chalmers University of Technology, Göteborg, Sweden.

Klein, P., and Vogel, H. 1993. Computer tomography — a help for dendrochronology and wood identification? *In* Proceedings of the 4th International Conference on Nondestructive Testing of Works of Art, Berlin, Germany. Deutsche Gesellschaft für Zerstörungsfreie Prüfung e. V., Berlin, Germany. pp. 85–91.

Kozakiewicz, P., and Gawarecki, K. 2003. Examination of historical wood internal structure using Roentgen-ray computed tomography. Ann. Warsaw Agric. Univ. For. Wood Technol. **53**: 223–227.

Lacroute, P., and Levoy, M. 1994. Fast volume rendering using a shear-warp factorization of the viewing transformation. *In* Proceedings of SIGGRAPH'94, Orlando, Florida, July 1994. pp. 451–458. Available from http://graphics.stanford.edu/papers/shear/.

Lemieux, H., Beaudoin, M., Zhang, S.Y., and Grondin, F. 2002. Improving structural lumber quality in a sample of *Picea mariana* logs sawn according to the knots. Wood Fiber Sci. **34**(2): 266–275.

Levi, C., Gray, J.E., McCullough, E.C., and Hattery, R.R. 1982. The unreliability of CT numbers as absolute values. Am. J. Roentgenol. **139**(3): 443–447. PMID:6981306.

Levoy, M. 1988. Display of surfaces from volume data. IEEE Comput. Graph. Appl. **8**(3): 29–37. doi:10.1109/38.511.

Li, P., Abbott, A.L., and Schmoldt, D.L. 1996. Automated analysis of CT images for the inspection of hardwood logs. *In* Proceedings of IEEE International Conference on Neural Networks. *Edited by* IEEE, Piscataway, N.J. pp. 1744–1749. Available from http://www.srs4702.forprod.vt.edu/PUBSUBJ/pdf/9604.pdf.

Lindgren, L.O. 1985. On the relationship between density / moisture content in wood and X-ray attenuation in computer tomography. *In* Proceedings of the 5th Symposium on Nondestructive Testing of Wood, Washington State University, Pullman, Wash. 9–11 September 1985. pp. 193–203. Luleå University of Technology, Luleå, Sweden.

Lindgren, L.O. 1988. Non-destructive measurements of density and moisture content in wood using computerized tomography. Tech. Lic. thesis, Royal Institute of Technology, Stockholm, Sweden. [In Swedish.]

Lindgren, L.O. 1991*a*. Medical CAT-scanning: X-ray absorption coefficients, CT-numbers and their relation to wood density. Wood Sci. Technol. **25**(6): 341–349.

Lindgren, L.O. 1991*b*. The accuracy of medical CAT-scan images for non-destructive density measurements in small volume elements within solid wood. Wood Sci. Technol. **25**(6): 425–432. doi:10.1007/BF00225235.

Lindgren, L.O., Davis, J., Wells, P., and Shadbolt, P. 1992. Non-destructive wood density distribution measurements using computed tomography. Eur. J. Wood Wood Prod. **50**(7-8): 295–299. doi:10.1007/BF02615356.

Longuetaud, F. 2005. Détection et analyse non destructive de caractéristiques internes de billons d'épicéa commun (*Picea abies* (L.) karst.) par tomographie à rayons X. Ph.D. thesis, École Nationale du Génie Rural des Eaux et Forêts, Unité associée INRA/ENGREF en Sciences Forestières.

Longuetaud, F., Leban, J.M., Mothe, F., Kerrien, E., and Berger, M. O. 2004. Automatic detection of pith on CT images of spruce logs. Comput. Electron. Agric. **44**(2): 107–119. doi:10.1016/j.compag.2004.03.005.

Longuetaud, F., Saint-André, L., and Leban, J.M. 2005. Automatic detection of annual growth units on *Picea abies* logs using optical and X-ray techniques. J. Nondestruct. Eval. **24**(1): 29–43. doi:10.1007/s10921-005-6658-8.

Longuetaud, F., Mothe, F., Leban, J.M., and Mäkelä, A. 2006. *Picea abies* sapwood width: variations within and between trees. Scand. J. For. Res. **21**(1): 41–53. doi:10.1080/02827580500518632.

Longuetaud, F., Mothe, F., and Leban, J.M. 2007. Automatic detection of the heartwood/sapwood boundary within Norway spruce (*Picea abies* (L.) Karst.) logs by means of CT images. Comput. Electron. Agric. **58**(2): 100–111. doi:10.1016/j.compag.2007.03.010.

Lorensen, W.E., and Cline, H.E. 1987. Marching cubes: a high resolution 3D surface construction algorithm. Comput. Graph. **21** (4): 163–169. doi:10.1145/37402.37422.

Lundgren, N., Hagman, O., and Johansson, J. 2006. Predicting moisture content and density distribution of Scots pine by microwave scanning of sawn timber II: Evaluation of models generated on a pixel level. J. Wood Sci. **52**(1): 39–43. doi:10.1007/s10086-005-0724-9.

Lüttschwager, D., Kätzel, R., and Löffler, S. 2004. Does the formation of heart wood indicate reduced vitality of pine trees (*Pinus sylvestris*)? Forstarchiv, **75**(5): 190–198.

Macedo, A., Vaz, C.M.P., Pereira, J.C.D., Naime, J.M., Cruvinel, P.

Can. J. For. Res. Downloaded from www.nrcresearchpress.com by UNIVERSITETSBIBLIOTEKET I TRONDHEIM on 09/18/12
For personal use only.

E., and Crestana, S. 2002. Wood density determination by X- and gamma-ray tomography. Holzforschung, **56**(5): 535–540. doi:10.1515/HF.2002.082.

Marčok, M., Kúdela, J., and Čunderlík, I. 1996. Identification of reaction beech wood by X-ray computed tomography. Eur. J. Wood Wood Prod. **54**(2): 97–98. doi:10.1007/s001070050145.

Meißner, M., Huang, J., Bartz, D., Mueller, K., and Crawfis, R. 2000. A practical evaluation of popular volume rendering algorithms. *In* Proceedings of the 2000 Volume Visualization Symposium, Salt Lake City, Utah, October 2000. pp. 81–90. Available from http://http://citeseerx.ist.psu.edu/viewdoc/summary?doi=10.1.1.140.1931 [accessed 31 May 2010].

Meyer-Spradow, J., Ropinski, T., Mensmann, J., and Hinrichs, K. 2009. Voreen: a rapid-prototyping environment for ray-casting-based volume visualizations. IEEE Comput. Graph. Appl. **29**(6): 6–13. doi:10.1109/MCG.2009.130.

Middleton, G.R., Alkan, S., Oja, J., Verret, D., and Munro, B.D. 2003. Utilizing CT log scanning to add value to British Columbia's forest estate: enabling software — Phase I. FPInnovations-Forintek Report to Forestry Innovation Investment, Recipient Agreement No. R2003-0135, April 2003. Forintek Canada Corporation, Québec, Qué

Moberg, L. 1999. Variation in knot size of *Pinus sylvestris* in two initial spacing trials. Silva Fenn. **33**(2): 131–144 Available from http://www.metla.fi/silvafennica/full/sf33/sf332131.pdf [accessed 31 May 2010].

Moberg, L. 2006. Predicting knot properties of *Picea abies* and *Pinus sylvestris* from generic tree descriptors. Scand. J. For. Res. **21**(S7): 49–61. doi:10.1080/14004080500487011.

Moberg, L., and Nordmark, U. 2006. Predicting lumber volume and grade recovery for Scots pine stems using tree models and sawmill conversion simulation. For. Prod. J. **56**(4): 68–74.

Morales, S., Guesalaga, A., Fernandez, M.P., Guarini, M., and Irarrazaval, P. 2004. Computer reconstruction of pine growth rings using MRI. Magn. Reson. Imaging, **22**(3): 403–412. doi:10.1016/j.mri.2004.01.015. PMID:15062936.

Mull, R. 1984. Mass estimates by computed tomography. Physical densities from CT-numbers. Am. J. Roentgenol. **143**: 1101–1104.

Müller, U., and Teischinger, A. 2001. Scanning-Technologien in der Holzwirtschaft [State of the Art-Report]. Holzforsch. Holzverwert. **53**(3): 53–56.

Niemz, P., Bodmer, H.C., Kucera, L.J., Ridder, H.W., Habermehl, A., Wyss, P., Zürcher, E., and Holdenrieder, O. 1998. Eignung verschiedener Diagnosemethodes zur Erkennung von Stammfäulen bei Fichte. Schweiz. Z. Forstwes. **149**(8): 615–630.

Nikolova, P.S., Blaschke, H., Matyssek, R., Pretzsch, H., Seifert, T., Rust, S., and Roloff, A. 2009. Combined application of computer tomography and light microscopy for analysis of conductive xylem area in coarse roots of European beech and Norway spruce. Eur. J. For. Res. **128**(2): 145–153.

Nordmark, U. 2002. Knot identification from CT images of young *Pinus sylvestris* sawlogs using artificial neural networks. Scand. J. For. Res. **17**(1): 72–78. doi:10.1080/028275802317221109.

Nordmark, U. 2003. Models of knot and log geometry of young *Pinus sylvestris* saw logs extracted from computed tomographic images. Scand. J. For. Res. **18**(2): 168–175. doi:10.1080/02827580310003740.

Occeña, L.G., and Schmoldt, D.L. 1996. GRASP — a prototype interactive graphic sawing program. For. Prod. J. **46**(11/12): 40–42.

Oja, J. 1997. A comparison between three different methods of measuring knot parameters in *Picea abies*. Scand. J. For. Res. **12**(3): 311–315. doi:10.1080/02827589709355415.

Oja, J. 2000. Evaluation of knot parameters measured automatically in CT-images of Norway spruce (*Picea abies* (L.) Karst.). Eur. J. Wood Wood Prod. **58**(5): 375–379. doi:10.1007/s001070050448.

Oja, J., and Temnerud, E. 1999. The appearance of resin pockets in CT-images of Norway spruce (*Picea abies* (L.) Karst). Eur. J. Wood Wood Prod. **57**(5): 400–406. doi:10.1007/s001070050368.

Oja, J., Grundberg, S., Fredriksson, J., and Berg, P. 2004. Automatic grading of sawlogs: a comparison between X-ray scanning, optical three-dimensional scanning and combinations of both methods. Scand. J. For. Res. **19**(1): 89–95. doi:10.1080/02827580310019563.

Okochi, T., Hoshino, Y., Fujii, H., and Mitsutani, T. 2007. Nondestructive tree-ring measurements for Japanese oak and Japanese beech using micro-focus X-ray computed tomography. Dendrochronologia, **24**(2–3): 155–164. doi:10.1016/j.dendro.2006.10.010.

Osterloh, K., Hasenstab, A., Zscherpel, U., Alekseychuk, O., Meinel, D., Goebbels, J., and Ewert, U. 2006. Radiographic and tomographic testing of wood. *In* Proceedings of the 9th European Conference on Non-Destructive Testing, Berlin, Germany, 25–29 September 2006. pp. 1–10. Available from http://www.ndt.net/article/ecndt2006/doc/Th.1.3.3.pdf [accessed 31 May 2010].

Osterloh, K., Bücherl, T., Hasenstab, A., Rädel, C., Zscherpel, U., Meinel, D., Weidemann, G., Goebbels, J., and Ewert, U. 2007. Fast neutron radiography and tomography of wood as compared to proton based technologies. *In* Proceedings of DIR 2007 — International Symposium on Digital Industrial Radiology and Computed Tomography, Lyon, France, 25–27 June 2007. pp. 1–12. Available from http://www.ndt.net/article/dir2007/papers/33.pdf [accessed 31 May 2010].

Pang, S., and Wiberg, P. 1998. Model predicted and CT scanned moisture distributed in a *Pinus radiata* board during drying. Eur. J. Wood Wood Prod. **56**(1): 9–14. doi:10.1007/s001070050256.

Panshin, A.J., and de Zeeuw, C.D. 1980. Textbook of wood technology. 4th ed. McGraw-Hill Book Company, New York.

Parker, M.L., and Jozsa, L.A. 1973. X-ray scanning machine for tree-ring width and density analysis. Wood Fiber Sci. **5**(3): 192–197.

Peter, R.K. 1962. Theoretical sawing of pine logs. For. Prod. J. **12**(11): 549–557.

Peter, R.K. 1967. Influence of sawing methods on lumber grade yield from yellow poplar. For. Prod. J. **17**(11): 19–24.

Petutschnigg, A.J., Flach, M., and Katz, H. 2002. Rotfäuleerkennung bei Fichte in CT-Bildern. Eur. J. Wood Wood Prod. **60**(3): 219–223. doi:10.1007/s00107-002-0287-z.

Pham, D.T., and Alcock, R.J. 1998. Automated grading and defect detection: a review. For. Prod. J. **48**(4): 34–42.

Radon, J. 1917. Über die Bestimmung von Funktionen durch ihre Integralwerte längs gewisser Mannigfaltigkeiten. Ber. Verh. Sächsische Akad. Wissenschaften **69**: 262–277.

Riedmiller, M., and Braun, H. 1993. A direct adaptive method for faster back-propagation learning: the RPROP algorithm. *In* Proceedings of IEEE International Conference on Neural Network, San Francisco, Calif., 28 March – 1 April 1993. pp. 828–845. Available from http://paginas.fe.up.pt/~ee02162/dissertacao/RPROP%20paper.pdf.

Rinnhofer, A., Petutschnigg, A., Andreu, J.P., Abbott, A.L., and Kline, D.E. 2003. Internal log scanning for optimizing breakdown. Comput. Electron. Agric. **41**(1–3): 7–21. doi:10.1016/S0168-1699(03)00039-5.

Rojas, G.E., and Ortiz, O.I. 2009. Identificación del cilindro nudoso en imágenes TC de trozas podadas de *Pinus radiata* utilizando el clasificador de máxima verosimilitud. Maderas Cienc. Technol. **11**(2): 117–127.

Rojas, G., Hernández, R.E., Condal, A., Verret, D., and Beauregard, R. 2005. Exploration of the physical properties of internal

Can. J. For. Res. Downloaded from www.nrcresearchpress.com by UNIVERSITETSBIBLIOTEKET I TRONDHEIM on 09/18/12
For personal use only.

characteristics of sugar maple logs and relationships with CT images. Wood Fiber Sci. **37**(4): 591–604.

Rojas, G.E., Condal, A., Beauregard, R., Verret, D., and Hernández, R.E. 2006. Identification of internal defect of sugar maple logs from CT images using supervised classification methods. Eur. J. Wood Wood Prod. **64**(4): 295–303. doi:10.1007/s00107-006-0105-0.

Rojas, G.E., Beauregard, R., Hernández, R.E., Verret, D., and Condal, A. 2007. Effect of moisture content variation on CT image classification to identify internal defects of sugar maple logs. For. Prod. J. **57**(4): 38–43.

Sandberg, K. 2006. Modelling water sorption gradients in spruce wood using CT scanned data. N.Z. J. For. Sci. **36**(2/3): 347–364.

Sarigul, E., Abbott, A.L., and Schmoldt, D.L. 2003. Rule-driven defects detection in CT images of hardwood logs. Comput. Electron. Agric. **41**(1–3): 101–119. doi:10.1016/S0168-1699(03)00046-2.

Schad, K.C., Schmoldt, D.L., and Ross, R.J. 1996. Nondestructive methods for detecting defects in softwood logs. U.S. For. Serv. Res. Pap. FPL-RP-546.

Schmoldt, D.L., Zhu, D., and Conners, R.W. 1993. Non-destructive evaluation of hardwood logs using automated interpretation of CT images. *In* Review of progress in quantitative non-destructive evaluation. Vol. 12. *Edited by* D.O. Thompson and D.E. Chimenti. Plenum Press, New York. pp. 2257–2264.

Schmoldt, D.L., Li, P., and Abbott, A.L. 1996. A new approach to automated labeling of internal features of hardwood logs using CT images. Rev. Prog. Quant. Nondestruct. Eval. **15**: 1883–1890.

Schmoldt, D.L., Occeña, L.G., Abbott, A.L., and Gupta, N. 1999. Non destructive evaluation of hardwood logs: CT scanning, machine vision and data utilization. Nondestruct. Test. Eval. **15**(5): 279–309. doi:10.1080/10589759908952876.

Schmoldt, D.L., He, J., and Abbott, A.L. 2000*a*. Automated labeling of log features in CT imagery of multiple hardwood species. Wood Fiber Sci. **32**(3): 287–300.

Schmoldt, D.L., Scheinman, E., Rinnhofer, A., and Occeña, L.G. 2000*b*. Internal log scanning: research to reality. *In* Proceedings of Annual Hardwood Symposium, Memphis, Tenn., 11–13 May 2000. pp. 103–114. Available from http://www.srs4702.forprod.vt.edu/pubsubj/pdf/00t21.pdf.

Seger, M.M., and Danielsson, P.-E. 2003. Scanning of logs with linear cone-beam tomography. Comput. Electron. Agric. **41**(1–3): 45–62. doi:10.1016/S0168-1699(03)00041-3.

Simpson, W.T. 1993. Specific gravity, moisture content, and density relationship for wood. U.S. For. Serv. Gen. Tech. Rep. FPL-GTR-76.

Sliwa, T., Brunet, P., Voisin, Y., Morel, O., Stolz, C., and Diou, A. 2003. Détection automatique des stries de croissance des arbres par transformée en ondelettes. *In* Proceedings of the 16th International Conference on Vision Interface, Halifax, Nova Scotia, 11–13 June 2003. pp. 376–381. Available from http://le2i.cnrs.fr/le2i/IMG/publications/Sliwa_169.pdf.

Som, S., Davis, J., Wells, P., and Svalbe, I. 1993. Morphology methods for processing tomographic images of wood. *In* Proceedings of Digital Image Computing: Techniques and Applications (DICTA), Sydney, Australia, 8–10 December 1993. Australian Pattern Recognition Society, The University of Queensland, Australia. pp. 564–571.

Som, S., Svalbe, I., Davis, J., Grant, J., Gold, E., Tsui, K., and Wells, P. 1995. Internal scanning of logs for grade evaluation and defect location. *In* Proceedings of Digital Image Computing: Techniques and Applications (DICTA), Brisbane, Australia, 6–8 December 1995. Australian Pattern Recognition Society, The University of Queensland, Australia. pp. 408–413.

Taylor, A.J. 2006. Wood density determination in *Picea sitchensis* using computerised tomography: how do density measuments compare with measurements of pilodyn pin penetration? Honours thesis, University of Wales, Bangor.

Taylor, F.W., Wagner, F.G., Jr, McMillin, C.W., Morgan, I.L., and Hopkins, F.F. 1984. Locating knots by industrial tomography — a feasibility study. For. Prod. J. **34**(5): 42–46.

Temnerud, E. 1997. Formation and prediction of resin pockets in *Picea abies* (L.) Karst. Ph.D. thesis, Swedish University of Agricultural Sciences, Uppsala, Sweden. Acta Universitatis Agriculturae Sueciae - Silvestria, 26.

Temnerud, E., and Oja, J. 1998. A preliminary study on unbiased volume estimation of resin pockets using stereology to interpret CT-scanned images from one spruce log. Eur. J. Wood Wood Prod. **56**(3): 193–200. doi:10.1007/s001070050298.

Thawornwong, S., Occeña, L.G., and Schmoldt, D.L. 2003. Lumber value differences from reduced CT spatial resolution and simulated log sawing. Comput. Electron. Agric. **41**(1–3): 23–43. doi:10.1016/S0168-1699(03)00040-1.

Tognetti, R., Raschi, A., Béres, C., Fenyvesi, A., and Ridder, H.W. 1996. Comparison of sap flow, cavitation and water status of *Quercus petraea* and *Quercus cerris* trees with special reference to computer tomography. Plant Cell Environ. **19**(8): 928–938. doi:10.1111/j.1365-3040.1996.tb00457.x.

Tsai, C.M., and Cho, Z.H. 1976. Physics of contrast mechanism and averaging effect of linear attenuation coefficients in a computerized transverse axial tomography (CTAT) transmission scanner. Phys. Med. Biol. **21**(4): 544–559. doi:10.1088/0031-9155/21/4/006. PMID:972920.

Uner, B., Oyar, O., Var, A.A., and Altnta, O.L. 2009. Effect of thinning on density of *Pinus nigra* tree using X-ray computed tomography. J. Environ. Biol. **30**(3): 359–362. PMID:20120459.

Wagner, F.G., Taylor, F.W., Ladd, D.S., McMillin, C.W., and Roder, F.L. 1989. Ultrafast CT scanning of an oak log for internal defects. For. Prod. J. **39**(11/12): 62–64.

Wang, X. 1997. Log classification by single X-ray scans using texture features from growth rings. Lecture Notes in Computer Science, Springer, Berlin and Heidelberg. (Print) ISSN 0302-9743 pp. 1611–3349. [Online.] [Computer Vision — ACCV'98, 1352/1997. pp. 129–136. ISBN 978-3-540-63931-2.]

Wei, Q., Leblon, B., Chui, Y.H., and Zhang, S.Y. 2008*a*. Identification of selected log characteristics from computed tomography images of sugar maple logs using maximum likelihood classifier and textural analysis. Holzforschung, **62**(4): 441–447. doi:10.1515/HF.2008.077.

Wei, Q., Chui, Y.H., Leblon, B., and Zhang, S.Y. 2008*b*. Identification of log characteristics in computed tomography images using back-propagation neural networks with the resilient back-propagation training algorithm and textural analysis: preliminary results. Wood Fiber Sci. **40**(4): 620–633.

Wei, Q., Chui, Y.H., Leblon, B., and Zhang, S.Y. 2009*a*. Identification of selected internal wood characteristics in computed tomography images of black spruce: a comparison study. J. Wood Sci. **55**(3): 175–180. doi:10.1007/s10086-008-1013-1.

Wei, Q., Zhang, S.Y., Chui, Y.H., and Leblon, B. 2009*b*. Reconstruction of 3D images of internal log characteristics by means of successive 2D log computed tomography images. Holzforschung, **63**(5): 575–580. doi:10.1515/HF.2009.089.

Wei, Q., Zhang, S.Y., Chui, Y.H., and Leblon, B. 2010. Identification of log characteristics in computed tomography images of black spruce (*Picea mariana*) logs by means of maximum likelihood classifier. Int. J. Tomogr. Stat. **14**(S10): 68–82.

Weihs, U. 2001. Farbkerndiagnose am stehenden Elsbeerenstamm. Allg. Forst Z. Waldwirtschaft Umweltvorsorge, **6**: 268–270.

Wells, P., Som, S., and Davis, J. 1991. Automated feature extraction from tomographic images of wood. *In* Proceedings of Digital Image Computing: Techniques and Applications (DICTA), Melbourne, Australia, 4–6 December 1991. Australian Pattern Recognition Society, The University of Queensland, Australia. pp. 198–199.

Westover, L. 1990. Footprint evaluation for volume rendering. *In* Proceedings of SIGGRAPH'90. pp. 367–376. Available from http://n.ethz.ch/~kaeserd/download/sciviz/Westover90.pdf.

Wu, J., and Liew, D. 2000. A computer vision method for detection of external log cracks and pith in log cross-section images. *In* Proceedings of World Automation Congress: International Symposium on Intelligent Automation and Control (ISIAC), Maui, Hawaii, 11–16 June 2000. pp. 531–536.

Xu, Z.J., Ye, N., Wang, H.L., and Ding, J.W. 2005. The reconstruction of log CT images of 3-D data using cubic natural spline function. J. Nanjing For. Univ. **29**(6): 132–134.

Yu, L., and Qi, D.W. 2008. Analysis and processing of decayed log CT image based on multifractal theory. Comput. Electron. Agric. **63**(2): 147–154. doi:10.1016/j.compag.2008.02.003.

Zhu, D.P., Conners, R.W., Schmoldt, D.L., and Araman, P.A. 1996. A prototype vision system for analyzing CT imagery of hardwood logs. IEEE Trans. Syst. Man Cybern. **26**(4): 522–532. doi:10.1109/3477.517028. PMID:18263051.

zu Castell, W., Schrödl, S., and Seifert, T. 2005. Volume interpolation of CT images from tree trunks. Plant Biol. **7**(6): 737–744. doi:10.1055/s-2005-872817. PMID:16388478.

Can. J. For. Res. Downloaded from www.nrcresearchpress.com by UNIVERSITETSBIBLIOTEKET I TRONDHEIM on 09/18/12
For personal use only.